HHS Public Access

Author manuscript

Anal Chim Acta. Author manuscript; available in PMC 2020 July 11.

Published in final edited form as:

Anal Chim Acta. 2019 July 11; 1061: 13–27. doi:10.1016/j.aca.2019.01.034.

High bandwidth approaches in nanopore and ion channel recordings – A tutorial review

Andreas J.W. Hartel[1,*], **Siddharth Shekar**[1], **Peijie Ong**[1], **Indra Schroeder**[2], **Gerhard Thiel**[2], **Kenneth L. Shepard**[1]

[1]Bioelectronic Systems Lab, Department of Electrical Engineering, Columbia University, New York City, 10027 - NY, US

[2]Plant Membrane Biophysics, Technische Universität Darmstadt, Darmstadt, Germany

Abstract

Transport processes through ion-channel proteins, protein pores, or solid-state nanopores are traditionally recorded with commercial patch-clamp amplifiers. The bandwidth of these systems is typically limited to 10 kHz by signal-to-noise-ratio (SNR) considerations associated with these measurement platforms. At high bandwidth, the input-referred current noise in these systems dominates, determined by the input-referred voltage noise of the transimpedance amplifier applied across the capacitance at the input of the amplifier. This capacitance arises from several sources: the parasitic capacitance of the amplifier itself; the capacitance of the lipid bilayer harboring the ion channel protein (or the membrane used to form the solid-state nanopore); and the capacitance from the interconnections between the electronics and the membrane. Here, we review state-of-the-art applications of high-bandwidth conductance recordings of both ion channels and solid-state nanopores. These approaches involve tightly integrating measurement electronics fabricated in complementary metal-oxide semiconductors (CMOS) technology with lipid bilayer or solid-state membranes. SNR improvements associated with this tight integration push the limits of measurement bandwidths, in some cases in excess of 10 MHz. Recent case studies demonstrate the utility of these approaches for DNA sequencing and ion-channel recordings. In the latter case, studies with extended bandwidth have shown the potential for providing new insights into structure-function relations of these ion-channel proteins as the temporal resolutions of functional recordings matches time scales achievable with state-of-the-art molecular dynamics simulations.

Graphical Abstract

*Correspondence should be addressed to hartel@ee.columbia.edu.

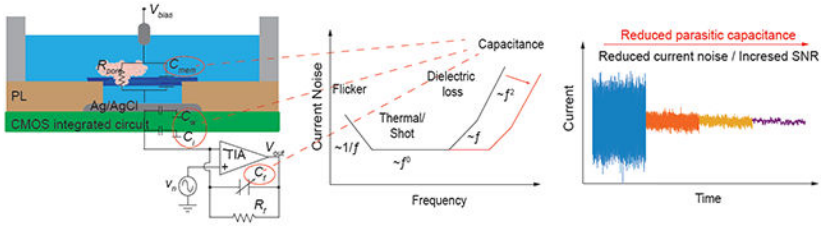

Keywords

Patch-clamp recordings; solid-state nanopores; lipid bilayer; ion channel recordings; integrated electronics; complementary metal-oxide semiconductors

1. Introduction

The function of ion-channel proteins is vital to many cellular processes, such as metabolism, energy harvesting, propagation of neuronal signals, and host-pathogen interactions. Aberrant channel behaviors often cause pathological conditions [1], and ion channels are a common drug target. In addition, as biomimetic leak channels, solid-state nanopores are also of increasing interest in modern diagnostic and bio-sensing studies.

Conductance of both ion channels and nanopores are measured with voltage-clamp amplifiers. These amplifiers ”clamp” the voltage between two terminals and measure the current. The ionic current signal is typically transduced into an electrical current through silver/silver-chloride (Ag/AgCl) electrodes. These electrodes are immersed in two buffer-filled compartments, which are separated by a chemically stable, ion-impermeable membrane (e.g. polytetrafluoroethylene or silicon nitride). In this manner, the flow of ions producing a measurable current is restricted to the single ion channel protein or nanopore of interest integrated into the membrane. In the absence of fluctuations of the channel conductance (e.g. due to ion-channel gating), the flow of ions is controlled by an electrochemical potential difference (V_{pore}), which can be created by any salt concentration gradient or electrical potential across the membrane. The ionic current (ΔI_{pore}) is the flux of ions from one compartment to the other in response to this electrochemical potential and is converted to an electrical current at the Ag/AgCl electrode interface. This electrical current is then converted to a voltage by a voltage-clamp amplifier, passed through an anti-aliasing filter, digitized, and, if needed, further digitally filtered to improve the signal-to-noise ratio (SNR) for band-limited signals.

The temporal resolution of such recordings is typically limited to microsecond time-scales depending on the properties of the patch-clamp amplifier and the channel itself. On the other hand, single-file translocations of ions are inherently faster, and depending on the conductance of the pore, correspond to nanosecond time-scales. For example, the time required for a monovalent ion to pass through an ion channel with a conductance of 100 pS at a potential of 100 mV is ~15 ns, making the temporal resolution of conventional patch-clamp amplifiers insufficient to resolve the smallest time scales of ion translocation dynamics.

2. Bandwidth limitations for voltage-clamp conductance measurements

In this section, we will consider the factors determining the temporal resolution of a voltage-clamp measurements of an ion channel or nanopore.

2.1 Signal-to-noise, noise and parasitic capacitance

The temporal resolution, which is inversely related to the maximum recording bandwidth (B_{max}) in voltage-clamp recordings, is limited by the required signal-to-noise ratio (SNR). The SNR in these recordings is defined as the ratio of the signal current amplitude defining state transitions (ΔI_{pore}) to the root-mean-square (RMS) current noise of the system (I_{noise}); $SNR = \frac{\Delta I_{pore}}{I_{noise}}$ (see Figure 1A). Typically, a SNR greater than three is sufficient for basic analysis of currents through channels, defining well-separated current level states in the channel. In the case of ion channels, this is typically the open and closed state of the protein, while for nanopores, this is the open and blocked state of the pore indicating the presence or absence of a translocating molecule. Other more-closely-spaced states may also be important, putting even more stringent requirements on noise levels.

Improvement of the SNR can be achieved either by increasing ΔI_{pore} or by reducing I_{noise}. ΔI_{pore} typically has a linear response to the applied potential V_{pore} and is characterized by the channel conductance G_{pore}. The latter can be influenced by factors such as the channel diameter and length, the salt concentration of the electrolyte, the charge of the conducting ions, and the temperature of the system [2-4]. The largest value of V_{pore} that can be applied is dependent on the experimental system in use. For solid-state nanopores, V_{pore} can be as high as 1 V, limited by hydrolysis of water; in experiments with lipid bilayers, V_{pore} is typically limited to 200-300 mV by the electroporation potential of the lipid bilayer [5].

I_{noise} is dominated by different noise sources depending on frequency. Figure 1B shows a qualitative plot of the input-referred current noise spectrum for a measurement platform consisting of a patch-clamp amplifier and a channel of interest. The shape of the noise spectrum results from the combination of several different noise sources, each having a frequency regime in which they are dominant. At low frequencies, the noise spectrum is dominated by the flicker noise, or 1/f, noise, of the channel itself (see Figure 1B). The flicker noise power spectral density (A^2/Hz) is given by $S_{I,\,flicker} = \frac{A \cdot \Delta I_{pore}^2}{f^{\beta}}$, where A is the normalized noise amplitude, f is the frequency, ΔI_{pore} is the current through the pore and $\beta \approx 1$ [6]. Flicker noise is generally attributed to fluctuations due to charge trapping or charge scattering. Flicker noise has been measured in both ion channels and solid-state nanopores [7, 8].

Beyond the flicker noise corner frequency (denoted as f_1 in Figure 1B), the noise is white, due to Johnson noise contributed by both the channel and the voltage-clamp amplifier. The RMS thermal noise from the channel conductance is given by $S_{I,\,thermal} = \frac{4k_BT}{R_{pore}}$ where R_{pore} is the resistance of the channel, k_B is the Boltzmann constant and T is temperature. The

amplifier also contributes thermal noise $S_{I,amp\,thermal} = \frac{4k_BT}{R_{feedback}}$ and represents the noise floor of the system, where $R_{feedback}$ is the feedback resistance of the amplifiers. The spectrum reaches another noise corner at f_2. Here, the noise spectrum often has a region of f-dependence, which can be attributed to one of two sources. The first is attributed to dielectric losses in the membrane; this dissipation is frequency dependent and the resulting f-dependent noise is given by $S_{I,f} = 8\pi k_B TDC_{total} f$ where D is the dielectric loss coefficient [6, 10]. Another source of the f noise is input-referred *voltage* flicker noise from the amplifier $S_{V,flicker} = \frac{A_{amp}}{f}$, where A_{amp} is the un-normalized input-referred voltage noise amplitude, applied across the total capacitance at the amplifier input (C_{total}) resulting in a current noise power spectral density $S_{I,f} = 4\pi^2 A_{amp} C_{total}^2 f$ [9]. At the highest frequencies, beyond the third corner frequency f_3, the noise spectrum begins to have an f^2 dependence. This f^2 noise results from the input-referred voltage noise of the amplifier (v_n) applied across C_{total}, ($S_{I,f^2} = 4\pi^2 f^2 C_{total}^2 v_n^2$).

The total input-referred current noise (I_{noise}) of the system, as shown in Figure 1B, can be calculated as,

$$I_{noise} \approx \sqrt{\int_0^{B_{max}} (S_{I,amp\,thermal} + S_{I,flicker} + S_{I,thermal} + S_{I,f} + S_{I,f^2}) df}.$$

At high B_{max} frequencies, typically greater than 10 kHz, the f^2 noise dominates and $B_{max} \propto \left(\frac{I_{pore}}{v_n C_{total}}\right)^{2/3}$ [9]. Improving B_{max} requires reducing C_{total} or the amplifier's v_n, as shown in Figure 1C. C_{total} is the sum of the capacitance at the input of the amplifier (C_{amp}), the capacitance of the lipid-bilayer or solid-state membrane (C_{mem}), and the capacitance of any interconnections between the electronics and the pore (C_w).

In summary, to achieve the highest possible bandwidth (i.e. the highest temporal resolution) at a given SNR the measurement platform must be optimized to deliver the highest signal amplitudes while reducing the current noise as much as possible. While signal amplitudes may be limited intrinsically, the measurement system can be optimized to reduce noise by improvements to the measurement electronics and reductions in parasitic capacitance.

2.2 High bandwidth approaches

The most commonly used patch-clamp amplifiers, such as the HEKA EPC-series and the Axopatch 200B [11-13], use a transimpedance amplifier architecture with either resistive (HEKA EPC-series) or capacitive feedback with active cooling of the head stage (Axopatch); the actively cooled head stage helps to lower the thermal noise floor of the amplifier. The amplifier head stage of both these systems are realized using discrete components, which are chosen to improve noise performance such as through the use of junction field-effect transistors, which can lower the flicker noise of the amplifier [14] [13]. In the case of the Axopatch 200B, which also has the noise advantages of capacitive

feedback, these techniques achieve an input-referred root-mean-squared (RMS) current noise of only 30 fA over the 0.1 - 100 Hz band [15]. Nonetheless, systems that use capacitive feedback architectures are generally limited in terms of their operating bandwidth by amplifier stability considerations. Furthermore, the input capacitance for these amplifiers is also typically greater than 15 pF [16].

Because of these considerations, the maximum bandwidth of conventional patch-clamp amplifiers is limited to approximately 100 kHz. These limitations can be partly overcome with aftermarket modifications of the amplifier head stage and pipette holders [17, 18]. However, even in these cases, achievable bandwidths become limited by C_{total} values, which can typically exceed 20 pF in these measurement systems [9].

Recent developments deploying measurement electronics developed in complementary metal-oxide semiconductors (CMOS) technology and tightly integrated with the channel under study have allowed for significant reductions in C_{total} to as low as 3 pF [4, 9, 19]. In addition to the reduction of C_{total}, the CMOS amplifiers can be designed to produce ν_n as low as 2.6 nV/(Hz)$^{1/2}$, comparable to commercial amplifiers [4]. This combination of reduced C_{total} and ν_n can improve achievable B_{max} values at a given SNR from ~10 kHz to as high as 10 MHz depending on the achievable ΔI_{pore} values [4]. A 10-MHz bandwidth corresponds to a temporal resolution of approximately 100 ns.

For ion-channel recordings, the choice of lipids affects the thickness of the membrane and its dielectric constant, with specific capacitances ≈ 0.5 μF/cm^2 being typical [9]. Reducing the membrane area is key to reducing C_{mem} [20]. Microfabrication techniques can be used to pattern the negative photoresist SU-8 into microwells which can be formed directly on top of the CMOS amplifier chips with a defined height and diameter [21, 22]. A well with a 30-μm diameter and 6-μm height has a volume of approximately 4 pL, opening the possibility of controlled experiments with very small concentrations or absolute number of analytes [19]. A nM concentration of analytes in this small chamber corresponds to only a few thousand molecules. With more advanced microfabrication methods, even smaller wells are possible [23]. This tight integration allows C_{total} to be reduced to as little as 3 pF for 20-μm-diameter membranes [16].

3. Biological and solid-state nanopores

The earliest documentation of the concept of nanopore DNA sequencing can be traced back to David Deamer's notebook from 1989 [24]. A nanopore is a nm-sized opening in a suspended membrane, which can be a lipid bilayer or other copolymer membrane in the case of biological pores or a dielectric membrane in the case of solid-state pores.

Biological nanopores are either protein toxins that form nanoscale pores or protein channels from the outer membrane of bacteria [25]. Early work focused on the use of α-hemolysin [26, 27], a naturally occurring protein channel secreted by the bacterium *Staphylococcus aureus*, but several other proteins have been subsequently explored including *Mycobacterium smegmatis* porin A (MspA) [28, 29], and *Escherichia coli* Outer membrane protein G (OmpG) [30]. The greatest advantage of biological nanopores comes from their

highly reproducible pore structure, which can also be engineered [31] to modulate various aspects of the pore such as the number of charges in the channel [28] or to introduce either reactive amino acids or hydrophobic groups that bind organic molecules [32].

While biological nanopores offer reproducibility, they lack chemical and mechanical stability, which may be required in some applications [33]. Solid-state nanopores, formed in dielectric membranes such as silicon nitride, address these issues [33, 34]. Microfabrication techniques developed for the electronics industry over the last few decades can be directly applied to create these pores. Reproducibility and scalability, however, continue to remain challenges to overcome for solid-state nanopores [35]. Further, translocation rates, at least for DNA analytes, is higher in solid-state nanopores by several orders of magnitude compared to biological nanopores, exacerbating the bandwidth limitations in conventional measurement approaches [36]. Indeed, the only commercial nanopore-based DNA sequencing technology as of the writing of this article uses arrays of biological nanopores [37]. Glass nanopipettes [38-40] are also a relatively low-cost and easy-to-manufacture form of solid-state nanopore at the cost of significantly higher access resistances. Furthermore, nanopipettes are only useful for experiments that require pores no smaller than a few 10's of nm.

Considering a cylindrical nanopore with diameter d and thickness t, the open-pore conductance of a nanopore [41] suspended in a solution with conductance σ, is given by

$$G_{open} = \sigma\left(\frac{4t}{\pi d^2} + \frac{1}{d}\right)^{-1}$$

where the first term represents the classical cylindrical conductor and the second term represents the contribution of the access resistance to the pore [42], which becomes of greater importance for pores when $\frac{d}{t} \ll 1$. As an analyte translocates through the pore, it modulates the pore conductance to $G_{blocked}$ [41] which can be expressed as

$$G_{blocked} = \sigma\left(\frac{4t}{\pi d_{eff}^2} + \frac{1}{d_{eff}}\right)^{-1}$$

with $d_{eff} = \sqrt{d^2 - d_{molecule}^2}$ representing the diameter of the translocating analyte. As shown in Section 2.1, a larger signal current is essential for achieving high bandwidth recordings [9]. Since $\Delta I_{pore} = V_{bias}(G_{open} - G_{blocked})$, it is desirable to apply larger bias voltages in order to maximize the signal. A larger bias voltage is also known to increase the capture rate [43]. However, these benefits come at the expense of decreased translocation times due to the relatively stronger electric field experienced by the analyte in the pore [44].

Both biological and solid-state nanopores have been used extensively in a variety of experiments. Perhaps the most popular use of nanopores has been in translocating and studying both single-stranded [4, 45] and double-stranded DNA [9, 44] molecules. Recently, homopolymer differentiation has been shown using solid-state nanopores [45, 46], and full

DNA sequencing is now possible using biological nanopores [37]. Due to the advent of high-bandwidth recording electronics, there is also an interest in studying protein translocations with the ultimate goal of achieving protein sequencing [47]. Nanopores have also been used to detect combinations of DNA and proteins such as DNA-protein complexes [48] and protein-protein complexes [49]. Beyond simple detection, nanopores are tools to study fundamental properties of biomolecules such as the equivalent charge per DNA base pair [50], the force [50] and velocity [51] profile experienced by DNA molecules in the pore, the force required to unzip DNA hairpins [52, 53], the preferred orientation of RNA molecules translocating through the pore [54], and sub-Å motor protein measurements [55].

This section explores the current state-of-the-art for biological and solid-state nanopores. We also discuss the benefits that tight integration with electronics can offer for nanopore studies.

3.1 State-of-the-art methods

Biological nanopores are usually inserted into a lipid membrane as shown in Fig. 2A. When the pore is blocked, for example by a DNA molecule, the current decreases such that the blocked current is a measure of the length and size of the DNA molecule. In addition to α-hemolysin and its engineered variants, transmembrane proteins such as MspA [28, 29] (Figure 2B), bacteriophage phi29 DNA-packaging motor [56], bacteriophage SPP1 DNA-packaging motor [57], *Escherichia coli* Fragaceatoxin C (FraC) [58], OmpG [30], *Escherichia coli* cytolysin A (ClyA) [59], *Escherichia coli* Curlin sigma S-dependent growth subunit G (CsgG) [60, 61] and aerolysin [62, 63] have been used as biological nanopores. Many of these pores have been specifically engineered for nanopore applications, for example, by removing negative charges from MspA [28] despite some controversy over the need for this enhancement [61].

Silicon nitride and silicon dioxide were among the first materials exploited for creating solid-state nanopores. The first technique to enable true nm-scale control over nanopore fabrication was the use of a focused ion beam [64]. Since then, fabrication by ablating material with a transmission electron microscope (TEM) has become equally popular [65]. The latest addition to the list of techniques for nanopore fabrication is controlled dielectric breakdown (Figure 3A) [66]. In this technique, a controllable voltage is applied across a pristine membrane and the current across the membrane is monitored. As the applied voltage increases, defect sites in the membrane allow charge to tunnel through the membrane which slowly erodes the surrounding region resulting in the creation of a nanopore [66]. Precise control over the voltage then allows for controlling the shape of the newly-created pore. Compared to the prevailing techniques, this method has advantages of cost-effectiveness and easy accessibility – requiring only a voltage source and a sensitive ammeter.

Since the thickness of the nanopore plays a crucial role in determining its spatial resolution, two-dimensional (2D) materials have emerged as an alternative to thinning conventional dielectric membranes. Indeed, as a single atomic layer, these materials represent the physical limit in membrane thickness. Graphene (Figure 3B) [67, 68], MoS_2 [69], hexagonal boron nitride (h-BN) [70] and WS_2 [71] have all been used to fabricate 2D nanopores. Unlike the amorphous films that result when conventional dielectrics are thinned [72] the crystalline

structure of these materials allows for fine-tuned control over nanopore diameter to sub-nm precision [70].

Both biological [37, 73] and solid-state nanopores [74, 75] have also been fabricated in arrays in order to enable high-throughput experiments. Dual nanopore configurations have allowed for the “indefinite” capture of a DNA molecule through a technique known as “DNA flossing”, where the molecule is moved back and forth between the two pores with independent bias voltages applied across each pore (Figures 3C,D) [76, 77].

3.2 Reducing membrane capacitance in nanopore recordings

As described in Section 2.1, noise at high bandwidths is determined primarily by the input-referred voltage noise of the amplifier shaped by the capacitance at the input of the amplifier, which is usually dominated by the capacitance of the membrane itself [9]. The capacitance of a simple parallel plate capacitor is given by

$$C = \frac{\epsilon A}{d}$$

where A is the area of the membrane and d is the thickness of the membrane. For experiments with biological pores in suspended lipid bilayers, the ability to control d is limited. As a result, the primary way to reduce C_{mem} in these experiments is by reducing the size of the membrane itself. An interesting approach to decreasing A has been to create a suspended lipid bilayer at the tip of a glass pipette (Figure 4A) [78]. This mimics the cell-attached patch-clamp setup used for recording ion channels in cell membranes. It is important to note, however, that the probability of channel incorporation varies inversely to the membrane area.

The membrane capacitance for solid-state nanopores is typically reduced by patterning and increasing the thickness of the membrane in the regions surrounding the pore by adding materials such as poly(dimethylsiloxane) (PDMS) [7] and SiO_2 (Figure 4B) [79, 80]. While devices without any additional dielectrics can have capacitances as large as 300 pF [7], the use of these techniques has allowed this number to be reduced to less than 1 pF [79]. Nanopipettes, with their thick glass walls, also are an attractive option when low membrane capacitance is required. Glass pipettes can also be combined with regular nanopores in order to have a μm sized droplet connected to the pore (Figure 4C) [81]. This currently represents the lowest capacitance achieved in nanopore recordings with $C_{mem} < 70$ fF [81].

3.3 CMOS-integrated approaches

While the total capacitance at the input of the amplifier is typically dominated by the membrane capacitance, other sources of capacitance such as the wiring capacitance and the input capacitance of the amplifier itself can become important as the membrane capacitance is reduced to sub-pF levels. For example, coaxial cables are commonly used as connections to amplifier inputs because they shield the signal wire from external electromagnetic interference. However, these cables have a capacitance to the shield (which is usually grounded) of ≈ 1 pF/cm. Recent efforts have introduced techniques to incorporate the

fluidics directly on top of custom-designed amplifiers, which can reduce the wiring capacitance down to less than 1 pF (Figure 4D) [9].

Custom-designed CMOS amplifiers have the added advantage of being able to reduce the amplifier input capacitance. Off-the-shelf amplifiers typically use discrete components assembled on a PCB in their head stages, which increases the capacitance at the input of the amplifier due to the large size of these devices and the associated parasitic capacitances of the packaging. Several recent efforts have shown that transimpedance amplifiers (TIAs) designed in conventional CMOS processes can achieve competitive noise performance to those of commercial discrete systems [4, 82-84]. Further, since these amplifiers are designed in advanced technology nodes with small feature sizes, the amplifier's input capacitance can be reduced to less than 1 pF [4, 9]. In addition to improved signal fidelity, CMOS integration aids the development of large, parallel nanopore arrays[73, 85].

The combination of low-noise electronics and reduced membrane and wiring capacitances along with ultra-thin solid-state nanopores have extended measurement bandwidths comfortably into the MHz regime [4, 9, 79]. For biological nanopores, which have current levels that are typically a factor of 100 lower, bandwidths as high as 200 kHz are theoretically possible. Analyte translocations are fast (for DNA, typically 10 μs/base for biological nanopores and 100 ns/base for solid-state nanopores [9, 27]) and require mechanisms to slow down this rate such as the use of a polymerase to ratchet the DNA [86] or the use of temperature [87] or concentration gradients [88]. Improving the measurement bandwidth can help eliminate the need for slow-down techniques and improve the error rate associated with these techniques. Improvements in measurement bandwidth can also be traded off for improvements in SNR at lower bandwidths.

4. Ion channel recordings

Single ion channel recordings are widely used, for example, in studies of structure-function relationships or of pharmacological responses [10, 89-92].

4.1 State-of-the-art methods

Typically, the conductance of ion channels is studied using heterologous expression of the proteins in cell lines such as human embryonic kidney (HEK) 293 and patch-clamping the cells [93-96]. The introduction of fire-polished capillaries with tip diameters of 0.5 – 1 μm (Figure 5A) allows analysis of ionic currents produced by individual ion channel proteins [96, 97]. These recordings enabled the detailed characterization of gating kinetics at the single-channel level [93, 94]. Patch-clamp methods have been noticeably improved by the development of the suction pipette holder, allowing the seal resistance to be increased and reducing the associated current noise [98]. Amplifier systems have been developed supporting bandwidths as high as 100 kHz for studying the dynamics of ion channel gating [11-13, 99].

As explained in Section 2.1 and 2.2, in a typical patch-clamp experiment, the maximum achievable bandwidth is limited by both the product of the total capacitance at the input of the amplifier (C_{total}) and the voltage noise (ν_n) at the input of the transimpedance amplifier.

Many approaches have been used to reduce the constituents to C_{total} such as the use of custom-made pipette holders to reduce C_w [17], the use of nano-pipettes (see Figure 5B) to reduce C_{mem} [100-102], and the use of amplifiers with lower input capacitance [17, 18]. By using integrated patch-clamp amplifier systems (Figure 5C and D) the contributions of C_{amp} and C_w can be reduced in same manner as was done for nanopore measurements to make C_{mem} the largest capacitive component [16, 19, 103]. Values for the specific membrane capacitance range from 0.7 to 1.3 μF/cm^2 depending on the lipid composition of the lipid bilayer [104] and the cell-type used [105].

Suspended lipid bilayers, often called black lipid membranes (BLM) due to their appearance under a light microscope, offer an extremely robust platform to study single-ion-channel gating under precisely controlled conditions. Most commonly, BLMs are prepared on openings in polytetrafluoroethylene (PTFE) chambers with a diameter of 100 to 300 μm resulting in a membrane capacitance in excess of 100 pF and limiting the bandwidth of the recordings to well below 10 kHz. Vertical or horizontal bilayers can be formed using various solvent and solvent-free methods from the solvent-water or air-water interface on the hydrophobic surfaces of the sample chamber [106-110]. Ion channels can be delivered by spontaneous incorporation of small proteins or peptides [111], from lipid nano-discs [112], or by fusion of liposomes containing the protein of interest [113]. The incorporation of liposomes is favorable in BLMs with larger diameters and becomes challenging in membranes with diameter below 30 – 50 μm [114].

Several studies have focused on the optimization of liposome fusion in suspended membranes [113]. Factors such as lipid compositions, charge of lipid head groups, presence of divalent cations (Ca^{2+} or Mg^{2+} when possible), salt concentration, lipid transition temperatures, and membrane viscosity can have an impact on the efficiency of liposome fusion [104, 115-117]. A salt gradient across the membrane is the most commonly used strategy creating an osmotic pressure difference across the membrane favoring vesicle fusion events [118]. Liposome fusion can be monitored by doping the lipids used for liposomes and BLMs with nystatin and ergosterol [119, 120]. During vesicle fusion, ergosterol and nystatin transiently form a local ionopore in the BLM which shows a characteristic current spike [119, 120]. Counting the current spikes using an ergosterol/nystatin control allows for the determination of the number of fused vesicles. When the number of integrated proteins per vesicle is known, this allows the determination of the number of integrated proteins per BLM. Conventional BLM setups allow for a wide variety of single-channel recordings with precise control of the experimental parameters, including transmembrane potential, pH, salt composition and concentration, and perfusion of channel regulators and inhibitors.

Several studies have focused on high-bandwidth recordings of ion channel proteins. To address the issue of SNR-limited bandwidth, these studies have typically focused on ion-channel proteins with high single-channel conductance such as BK channels, their bacterial homologous MthK, and the ryanodine receptors [121-123]. In addition to these channels, studies have been performed on the family of prototypical viral potassium channels Kcv. High-bandwidth recordings combined with analysis of the open-channel noise using model-based assumptions on the open-channel noise (for more detail see Section 4.4), have shown that the putative inactivation visible in the current/voltage curves (I-V) of single-channel

recordings arise from the artificial reduction of the current amplitude by the cut-off of the low-pass filter due to insufficient bandwidth in the recordings [124].

These bandwidths can be improved by reducing the capacitance associated with the lipid membrane itself, described in Section 4.2, and by employing approaches to integrate *in vitro* membranes directly with CMOS-integrated amplifiers, described in Section 4.3.

4.2 Reducing total capacitance in single-channel recordings

The bandwidth in single-channel recordings using BLMs with a diameter of 100 – 300 μm is limited by SNR to less than 10 kHz by the membrane capacitance, which is typically greater than 100 pF. Probably the smallest commercially available suspended membrane system is the 50-μm multi-electrode-chip-array (MECA) offered by Ionera [125, 126]. Other approaches can be employed for the preparation of lipid bilayers with diameters below 50 μm. The most commonly used approaches to prepare such BLMs for single-channel recordings are based either on using conventional patch pipettes or nano-pipettes [78, 127] or on using openings in planar substrates such as PTFE foil [106, 107] or other hydrophobic materials [22, 102, 128]. The greatest benefit of using conventional patch pipettes and nano-pipettes to prepare lipid membranes is the relatively straight-forward method of preparation using a capillary puller or laser puller [129]. Others have formed BLMs at the contact point of two bubbles, of a few tens of μm in size, filled with aqueous buffer. In an oil environment, added lipids form a monolayer around these bubbles, resulting in a bilayer at the contact point [112, 130].

BLMs on pipettes are very small (typically less than 1 μm in diameter) and consequently can have a very low membrane capacitance (as small as a few fF) [100, 101, 131, 132]. Incorporation of proteins into suspended membranes on pipettes is easily done for small, water-soluble pore-forming peptides but becomes more challenging for larger ion-channel proteins that require more elaborate incorporation strategies using liposomes [78, 131]. Delivery can be achieved by using proteins reconstituted in giant uni-lamellar vesicles (GUVs) and applying a negative pressure at the pipette. The GUVs are sucked onto the pipette tip and adhere and rupture to form a suspended bilayer spanning the tip of the pipette [78, 127]. However, BLMs with a diameter below 3 - 5 μm are known to show asymmetrical and artificial lipid pore currents due to pressure sensitivity and flexoelectricity, i.e. curvature-induced polarization, of low-radius membranes [133, 134].

Apertures for BLMs larger than 100 μm are far easier to fabricate but lead to considerably larger membrane capacitance. BLMs on this scale can easily be fabricated manually in hydrophobic substrates, such as PTFE or over-head plastic sheets perforated using a heated metal stylus or a sharp needle [128, 135]. For openings below 100 μm, manual preparation becomes difficult; however, substrates can be fabricated using photolithographic (PL) processes [16, 19, 22]. Here, the feature of choice is developed by UV exposure through a photo-mask onto a homogenous spin-coated layer of photo-resist. UV exposed areas become either soluble (positive-tone resist) or insoluble (negative-tone resist) to the subsequent chemical development process. UV-PL enables fabrication of structures with a minimal feature size typically on the order of 1 to 3 μm [23] and can be used with hydrophobic photoresists such as SU-8 (Michrochem). Structures patterned in SU-8 are hydrophobic and

allow the preparation of BLMs spanning micro cavities with a diameter of 20 – 30 μm reducing the membrane capacitance to as low as 1 pF [16, 19]. These and other approaches allow the combination of BLMs with planar electrodes as supporting structures and open up possibilities for various patch-on-a-chip strategies (Figure 6A) [22, 102, 103, 120, 136]. Furthermore, multi-membrane systems can be fabricated enabling multiple parallel experiments increasing the throughout put in single-channel recordings [137-139].

Reduction in the area of the lipid bilayer can be used to reduce the membrane capacitance below 1 pF. However, in this case, the wiring capacitance (C_w) and the capacitance of the amplifier (C_{amp}) often dominate the capacitance at the amplifier input. By tightly integrating the electronics and the lipid bilayer system, these capacitance components can also be reduced.

4.3 High bandwidth recordings using CMOS-integrated approaches

CMOS-integrated measurement electronics can be used in combination with lipid bilayers for the study of the gating mechanism of ion channel proteins at high temporal resolution [16, 19]. For this purpose, a micro-cavity with a diameter of 20 - 30 μm is directly fabricated into a hydrophobic photoresist layer on top of the integrated circuit (see Figure 6A and 6B). The hydrophobic photoresist layer is then used to form a lipid bilayer.

Miniaturization of the lipid bilayer and the tight integration with the measurement electronics implemented in CMOS reduces C_{total} from > 100 pF to as low as 4 pF [19]. Using this approach, it was possible to analyze the Ca^{2+}-dependent inactivation of the Type 1 Ryanodine receptor (RyR1) at a bandwidth of up to 500 kHz, equivalent to a temporal resolution of 2 μs at a SNR > 8 (Figure 6C). RyR1 is a Ca^{2+}-controlled Ca^{2+} release channel involved in the excitation-contraction coupling in skeletal muscle [140]. At low Ca^{2+}-concentrations, the channel is closed and activation is evoked by elevated Ca^{2+} and the channel is inactivated by Ca^{2+} in the mM range [141]. Analysis of channel dynamics at high bandwidth reveals increased close-channel flicker at intermittent Ca^{2+}-concentration. More interestingly, at inactivating Ca^{2+} concentrations, high bandwidth recordings at 500 kHz were able to identify two discrete close-state distributions in the dwell-time histograms, which were unidentifiable at bandwidth < 10 kHz achievable with conventional patch-clamp approaches (Figure 6D). The identification of two discrete close-state distributions in the dwell-time histogram supports the presence of an independent structural mechanism for the Ca^{2+}-dependent activation and inactivation mechanism of the RyR1 [19].

4.4 Increased effective bandwidth by data analysis

The most common analytical tool for the kinetics of single-channel recordings are dwell-time histograms [142] (Figure 6D). Here, an algorithm determines the transition times between the open and closed (or open and blocked) states and groups the resulting open and closed events by duration. Several techniques have been developed to improve the detection quality of these so-called jump detectors [143-146] and for correcting the data for missed events [147-151]. Typically, this improves the temporal resolution by a factor of two to four above the nominal bandwidth of the recording instrumentation. Another approach to improving the temporal resolution of these current traces is to fit them to a Markov model

using a maximum likelihood criterion [152-154]. The improvements achieved in the temporal resolution, however, are also quite limited [155].

Interestingly, the analysis methods with the highest temporal resolution are those that operate in the frequency domain. For example, analysis of the current power spectrum allowed resolution of the formamide block in gramicidin A channels with kinetics on a timescale of 100 ns. The corresponding data were recorded with only 20 kHz bandwidth [156]. With certain assumptions, these analysis methods are able to deliver temporal resolutions higher than the bandwidth limitations of the recordings.

Beta distributions are another method that can be used to analyze fast gating events and push the limits of temporal resolution in single-channel recordings. As shown in Figure 7A, information about the kinetics of interest can be lost due to the SNR-limited bandwidth and aggressive low-pass filtering [157, 158]. Instead of the true open-channel current and individual events, a reduced effective open current level and high open-channel noise is recorded due to the filtering of short closed-state events. In these cases, this closed state flickering can be inferred from the open-channel “noise.” In addition to the analysis of heavily filtered gating kinetics, beta distribution methods allow for the reconstruction of the true single-channel current amplitude (I_{true} in Figure 7A). The low-pass filtering of fast gating leads to specific distortions of the current amplitude distribution caused by the excess open channel noise (Figure 7B). By fitting these amplitude histograms, information about the underlying gating process and open channel current can be extracted [157]. The first implementations of this technique date back to the 1980s [159, 160]. This early work used an analytical expression for the histograms, the beta distribution function, and could, for example, resolve fast gating and block in K^+ channels [160-163] and ryanodine receptors [164]. An alternative approach models the amplitude histograms of channels with rapid kinetics with a sum of Gaussians [165].

Analytical techniques, such as the beta distribution, often rely on restrictive models, such as one with a single open and closed state and the assumption that the temporal response is governed by a first-order low-pass filter. More complex models can be accommodated with a simulation-based approach from model-derived differential equations [166-170]. To create these extended beta distribution, which can be applied to models with more than two states and more than one channel, a candidate Markov model [147, 171] with a set of rate constants and a single-channel current for the open state is used to simulate a series of current jumps in continuous time (Figure 7C). The simulated data are then filtered with a digital representation of the analog low-pass filter used in the experiment and subsequently sampled. An amplitude histogram is created from this filtered current time series. The baseline noise with the same current distribution as the experimental current trace can be added before or after construction of the amplitude histogram. The latter procedure is generally preferred since it requires less computing time. The theoretical amplitude histogram is in the next step fit to the histogram of the measured amplitudes using an optimization algorithm. The result of this analysis is a set of model parameters, including the open channel current and the rate constants of the Markov model [157]. Many other measurement features can be accommodated into these analyses, including sub-conducting states with different conductivities, digital filters of higher order (comparable to the filters

used in experimental setups), noise [172] including shot-noise and non-Gaussian sources. In this way, the kinetics of channel fluctuations can be reliably analyzed at effective temporal resolutions up to 20 times faster than that determined by the nominal bandwidth of the recording within the limitations of these models [121, 122, 173].

Extended beta distributions have been successfully applied to examine fast passage of an antibiotic through a bacterial porin [174] and fast gating in K^+ channels [121, 122, 175]. Further, the use of extended beta distributions allows quantitative modelling of the ion occupancies in the pore of a viral K^+ channel in a quantitative manner using the measured gating kinetics of the channel. This work demonstrated how voltage sensitivity in ion channels can be caused by the permeating ions without the presence of a specialized sensing domain [176]. The 'voltage sensor' in this case is an extracellular binding site in the Kcv_{NTS} channel; occupation of this binding site with K^+ stabilizes the open conformation, while depletion of K^+ leads to destabilization. The ability to determine the true open channel current from the heavily filtered data by beta extended distributions was crucial to the analysis.

The extended beta distribution has also been successfully applied as a post-recording analysis to the 500 kHz RyR1 recordings on the integrated CMOS platform. Two distinct closed states with time constants as brief as 300 and 35 ns could be described for RyR1. The effective on-rates of Ca^{2+} binding sites under the experimental concentration (0.03 – 400 μM) are typically in the range of 2.5 and 100 μs^{-1}. This means that the very fast channel dynamics are not directly due to the binding of Ca^{2+} but likely to subdomain movements in the filter region of RyR1 [19]. Additionally, the short time-scale of the conformational changes rules out entire domain or multi-domain movements as the mechanism.

5. Future perspectives and limitations of high bandwidth recordings

The detection of transition rates of ions in the ns-regime in the methodological frame-work of combined high bandwidth recordings and extended data analysis pushes the temporal resolution towards resolving single-file ion translocation events. Depending on the conductance of the ion channel, single-file translocation of an ion occurs in the order of 0.1–100 ns [177, 178]. These time scales are meanwhile easily accessible by computer-based molecular dynamics (MD) simulations.

The combination of increasingly longer MD simulations with the higher resolution of single-channel recordings is a promising future direction in the study of structure-function relationships in ion-channel proteins. To achieve this goal, a carefully tuned experimental approach is needed. Low-noise/high-bandwidth recordings require high single-channel current, I_{pore}, while the length of MD simulations is dependent on the computing power available and the number of atoms in the molecule of interest [179]. For the moment, the high bandwidth recording of RyR1 at a temporal resolution of 2 μs marks the fastest single ion channel recording achieved to date. These high bandwidth recordings are achievable because of the high conductance of RyR1 for potassium ions of up to 900 pS. While RyR proteins have this favorably large conductance they also have a molecular weight of up to 2

MDa, making them among the largest known ion channel proteins [180], rendering RyR1 a difficult model system for long MD simulations.

Further work is needed to improve the noise performance of CMOS-integrated voltage-clamp measurement electronics to achieve similarly high bandwidth recordings with smaller ion channel proteins of lower conductance. Good candidates are the prototypical viral K^+ channels of the Kcv family. These channels can be easily reconstituted into lipid bilayers [112], while having a relatively high unitary conductance (~100 pS) and a very small size (<100 amino acids) [181]. This should enable both high-temporal-resolution recordings and long MD simulations on the μs-timescale [179]. This opens a future possibility that molecular events, which are seen in the MD simulations, like the hopping of single ions through a selectivity filter [182], can be directly correlated with gating events resolved from electrical recordings.

Acknowledgements

This work was supported in part by the W. M. Keck Foundation and by the National Institutes of Health under Grants R01HG009189 and R01HG006879 to K.L.S.; the Landes-Offensive zur Entwicklung Wissenschaftlich-ökonomischer Exzellenz (LOEWE) initiative (iNAPO) and European Research Council (ERC) 2015 Advanced Grant 495 (AdG) n. 695078 414 noMAGIC to G.T.; and the Deutsche Forschungsgemeinschaft, SCHR 1467/1-1 to I.S.

References

[1]. Ashcroft FM, From molecule to malady, Nature, 440 (2006) 440–447. [PubMed: 16554803]

[2]. Kant K, Priest C, Shapter J, Losic D, The influence of nanopore dimensions on the electrochemical properties of nanopore arrays studied by impedance spectroscopy, Sensors (Basel, Switzerland), 14 (2014) 21316.

[3]. Kowalczyk SW, Wells DB, Aksimentiev A, Dekker C, Slowing down DNA translocation through a nanopore in lithium chloride, Nano letters, 12 (2012) 1038–1044. [PubMed: 22229707]

[4]. Shekar S, Niedzwiecki DJ, Chien C-C, Ong P, Fleischer DA, Lin J, Rosenstein JK, Drndic M, Shepard KL, Measurement of DNA translocation dynamics in a solid-state nanopore at 100 ns temporal resolution, Nano letters, 16 (2016) 4483–4489. [PubMed: 27332998]

[5]. Tung L, Trioano G, Sharma A, Raphael RM, Stebe KJ, Changes in electroporation thresholds of lipid membranes by surfactants and peptides, Acad of Sci, 888 (2006) 249–265.

[6]. Smeets RMM, Keyser UF, Dekker NH, Dekker C, Noise in solid-state nanopores, Proc Natl Acad Sci U S A, 105 (2008) 417–421. [PubMed: 18184817]

[7]. Tabard-Cossa V, Trivedi D, Wiggin M, Jetha NN, Marziali A, Noise analysis and reduction in solid-state nanopores, Nanotechnology, 18 (2007) 1–16.

[8]. Wohnsland F, Benz R, 1/f-Noise of open bacterial porin channels, J. Mem. Biol, 158 (1997) 77–85.

[9]. Rosenstein JK, Wanunu M, Merchant CA, Drndic M, Shepard KL, Integrated nanopore sensing platform with sub-microsecond temporal resolution, Nature Methods, 9 (2012) 487–492. [PubMed: 22426489]

[10]. Sakmann B, Neher E, Single-Channel Recording, Springer New York 2009.

[11]. Sigworth FJ, Design of the EPC-9, a computer-controlled patch-clamp amplifier. 1. Hardware, J. Neuroscience Meth, 56 (1995) 195–202.

[12]. Sigworth FJ, Affolter H, Neher E, Design of the EPC-9, a computer-controlled patch-clamp amplifier. 2. Software, J. Neuroscience Meth, 56 (1995) 203–215.

[13]. The Axon Guide, Electrophysiology and Biophysics Laboratory Techniques, Third Edition ed., MDS Analytical Technologies Sunnyvale, 2012.

[14]. Fleischer DA, Shekar S, Dai S, Field RM, Lary J, Rosenstein JK, Shepard KL, CMOS-Integrated Low-Noise Junction Field-Effect Transistors for Bioelectronic Applications, IEEE Electron Device Letters, 39 (2018) 931–934. [PubMed: 30666084]

[15]. Noise in electrophysiological measurements in: Sherman-Gold R (Ed.) The axon guide, electropysiology and biophysic laboratory techniques, Foster City 1993, pp. 235–264.

[16]. Rosenstein JK, Ramakrishnan S, Roseman J, Shepard KL, Single ion channel recordings with CMOS-anchored lipid membranes., Nano Let., 13 (2013) 2682–2686. [PubMed: 23634707]

[17]. Parzefall F, Wilhelm R, Heckmann M, Dudel J, Single channel currents at six microsecond resolution elicited by acetylcholine in mouse myoballs, J. Physiol, 512 (1998) 181–188. [PubMed: 9729627]

[18]. Shapovalov G, Gating transitions in bacterial ion channels measured at 3 μs resolution, J. Gen. Phys, 124 (2004) 151–161.

[19]. Hartel AJW, Ong P, Schroeder I, Giese MH, Shekar S, Clarke OB, Zalk R, Marks AR, Hendrickson WA, Shepard KL, Single-channel recordings of RyR1 at microsecond resolution in CMOS-suspended membranes, Proc Natl Acad Sci U S A, (2018) 201712313.

[20]. Sugawara M, Hirano A, Design and application of planar bilayer lipid membranes containing biological ion channels for chemical sensing, in: Tien HT, Ottova-Leitmannova A (Eds.) Advances in planar lipid bilayers and liposomes, Academic Press, Waltham, 2005, pp. 221–245.

[21]. Hirano-Iwata A, Oshima A, Kimura Y, Niwano M, Stable and reproducible bilayer lipid membranes based on silicon microfabrication techniques, Adv. Planar Lipid Bilayer and Liposomes ac.els-cdn.com2010, pp. 71–86.

[22]. Cheng Y, Bushby R, Evans S, Knowles P, Miles R, Ogier S, Single ion channel sensitivity in suspended bilayers on micromachined supports, Langmuir, 17 (2001) 1240–1242.

[23]. Altissimo M, E-beam lithography for micro-/nanofabrication, Biomicrofluidics, 4 (2010) 026503. [PubMed: 20697574]

[24]. Deamer DW, Akeson M, Branton D, Three decades of nanopore sequencing, Nature Biotech., 34 (2016) 518–524.

[25]. Cao C, Long YT, Biological nanopores: confined spaces for electrochemical single-molecule analysis, Accounts of Chemical Research, 51 (2018) 331–341. [PubMed: 29364650]

[26]. Kasianowicz JJ, Brandin E, Branton D, Deamer DW, Characterization of individual polynucleotide molecules using a membrane channel, Proc. Natl. Acad. Sci. U S A, 93 (1996) 13770–13773. [PubMed: 8943010]

[27]. Akeson M, Branton D, Kasianowicz JJ, Brandin E, Deamer DW, Microsecond time-scale discrimination among polycytidylic acid, polyadenylic acid, and polyuridylic acid as homopolymers or as segments within single RNA molecules, Biophys. J, 77 (1999) 3227–3233. [PubMed: 10585944]

[28]. Butler TZ, Pavlenok M, Derrington IM, Niederweis M, Gundlach JH, Single-molecule DNA detection with an engineered MspA protein nanopore, Proc. Natl. Acad. Sci. U S A, 105 (2008) 20647–20652. [PubMed: 19098105]

[29]. Manrao EA, Derrington IM, Pavlenok M, Niederweis M, Gundlach JH, Nucleotide discrimination with DNA immobilized in the MSPA nanopore, PLoS ONE, 6 (2011) e25723. [PubMed: 21991340]

[30]. Chen M, Khalid S, Sansom MSP, Bayley H, Outer membrane protein G: engineering a quiet pore for biosensing, Proc. Natl. Acad. Sci. U S A, 105 (2008) 6272–6277. [PubMed: 18443290]

[31]. Bayley H, Braha O, Cheley S, Gu L-Q, Engineered Nanopores, in: Fersht A (Ed.) Protein Science Encyclopedia, Wiley-VCH Verlag GmbH, United States, 2008.

[32]. Gu LQ, Braha O, Conlan S, Cheley S, Bayley H, Stochastic sensing of organic analytes by a pore-forming protein containing a molecular adapter, Nature, 398 (1999) 686–690. [PubMed: 10227291]

[33]. Rhee M, Burns MA, Nanopore sequencing technology: nanopore preparations, Trends Biotechnol., 25 (2007) 174–181. [PubMed: 17320228]

[34]. Dekker C, Solid-state nanopores, Nature Nanotechnol., 2 (2007) 209–215. [PubMed: 18654264]

[35]. Lee K, Park K-B, Kim H-J, Yu J-S, Chae H, Kim H-M, Kim K-B, Recent progress in solid-state nanopores, Advanced Materials, 10 (2018).

[36]. Venkatesan BM, Bashir R, Nanopore sensors for nucleic acid analysis, Nature Nanotech., 6 (2011) 615–624.

[37]. Loman N, The long view on sequencing, Nature Biotechnology, 36 (2018) 287.

[38]. Fraccari RL, Carminati M, Piantanida G, Leontidou T, Ferrari G, Albrecht T, High-bandwidth detection of short DNA in nanopipettes, Faraday Discuss., (2016) 1–15.

[39]. Bell NAW, Keyser UF, Digitally encoded DNA nanostructures for multiplexed , single-molecule protein sensing with nanopores, Nature Nanotech, (2016) 645–651.

[40]. Chen K, Bell NAW, Kong J, Tian Y, Keyser UF, Direction- and salt-dependent ionic current signatures for DNA sensing with asymmetric Nanopores, Biophys. J, 112 (2017) 1–15. [PubMed: 28076800]

[41]. Kowalczyk SW, Grosberg AY, Rabin Y, Dekker C, Modeling the conductance and DNA blockade of solid-state nanopores, Nanotech., 22 (2011) 315101.

[42]. Hall JE, Access resistance of a small circular pore, J. Gen. Phys, 66 (1975) 531–532.

[43]. Chen P, Mitsui T, Farmer DB, Golovchenko J, Gordon RG, Branton D, Atomic layer deposition to fine-tune the surface properties and diameters of fabricated nanopores, Nano Letters, 4 (2004) 1333–1337. [PubMed: 24991194]

[44]. Wanunu M, Sutin J, McNally B, Chow A, Meller A, DNA translocation governed by interactions with solid-state nanopores, Biophys. J, 95 (2008) 4716–4725. [PubMed: 18708467]

[45]. Venta K, Shemer G, Puster M, Rodríguez-Manzo JA, Balan A, Rosenstein JK, Shepard K, Drndic M, Differentiation of short, single-stranded DNA homopolymers in solid-state nanopores, ACS Nano, 7 (2013) 4629–4636. [PubMed: 23621759]

[46]. Akahori R, Yanagi I, Goto Y, Harada K, Yokoi T, Takeda K-I, Discrimination of three types of homopolymers in single-stranded DNA with solid-state nanopores through external control of the DNA motion, Scientific Reports, 7 (2017) 1–14. [PubMed: 28127051]

[47]. Restrepo-Pérez L, Joo C, Dekker C, Paving the way to single-molecule protein sequencing, Nature Nanotechnology, 13 (2018) 786–796.

[48]. Squires AH, Gilboa T, Torfstein C, Varongchayakul N, Meller A, Single-molecule characterization of DNA–protein interactions using nanopore biosensors, Methods in Enzymology, 582 (2017) 353–385. [PubMed: 28062042]

[49]. Freedman KJ, Bastian AR, Chaiken I, Kim MJ, Solid-state nanopore detection of protein complexes: Applications in healthcare and protein kinetics, Small, 9 (2013) 750–759. [PubMed: 23074081]

[50]. Keyser UF, Koeleman BN, Van Dorp S, Krapf D, Smeets RMM, Lemay SG, Dekker NH, Dekker C, Direct force measurements on DNA in a solid-state nanopore, Nature Physics, 2 (2006) 473–477.

[51]. Lu B, Albertorio F, Hoogerheide DP, Golovchenko JA, Origins and consequences of velocity fluctuations during DNA passage through a nanopore, Biophys. J, 101 (2011) 70–79. [PubMed: 21723816]

[52]. Dudko OK, Hummer G, Szabo A, Theory, analysis, and interpretation of single-molecule force spectroscopy experiments, Proc. Natl. Acad. Sci. U S A, 105 (2008) 15755–15760. [PubMed: 18852468]

[53]. Dudko OK, Mathé J, Szabo A, Meller A, Hummer G, Extracting kinetics from single-molecule force spectroscopy: Nanopore unzipping of DNA hairpins, Biophys. J, 92 (2007) 4188–4195. [PubMed: 17384066]

[54]. Butler TZ, Gundlach JH, Troll MA, Determination of RNA orientation during translocation through a biological nanopore, Biophys. J, 90 (2006) 190–199. [PubMed: 16214857]

[55]. Derrington IM, Craig JM, Stava E, Laszlo AH, Ross BC, Brinkerhoff H, Nova IC, Doering K, Tickman BI, Ronaghi M, Mandell JG, Gunderson KL, Gundlach JH, Subangstrom single-molecule measurements of motor proteins using a nanopore, Nature Biotech., 33 (2015) 1073–1075.

[56]. Wendell D, Jing P, Geng J, Subramaniam V, Lee TJ, Montemagno C, Guo P, Translocation of double-stranded DNA through membrane-adapted phi29 motor protein nanopores, Nature Nanotechnology, 4 (2009) 765–772.

[57]. Zhou Z, Ji Z, Wang S, Haque F, Guo P, Oriented single directional insertion of nanochannel of bacteriophage SPP1 DNA packaging motor into lipid bilayer via polar hydrophobicity, Biomaterials, 105 (2016) 222–227. [PubMed: 27529454]

[58]. Wloka C, Mutter NL, Soskine M, Maglia G, Alpha-helical fragaceatoxin C nanopore engineered for double-stranded and single-stranded nucleic acid analysis, Angewandte Chemie - International Edition, 55 (2016) 12494–12498. [PubMed: 27608188]

[59]. Soskine M, Biesemans A, De Maeyer M, Maglia G, Tuning the size and properties of ClyA nanopores assisted by directed evolution, J. Am. Chem. Soc, 135 (2013) 13456–13463. [PubMed: 23919630]

[60]. Goyal P, Krasteva PV, Van Gerven N, Gubellini F, Van Den Broeck I, Troupiotis-Tsaïlaki A, Jonckheere W, Péhau-Arnaudet G, Pinkner JS, Chapman MR, Hultgren SJ, Howorka S, Fronzes R, Remaut H, Structural and mechanistic insights into the bacterial amyloid secretion channel CsgG, Nature, 516 (2014) 250–253. [PubMed: 25219853]

[61]. Brown CG, Clarke J, Nanopore development at Oxford Nanopore, Nature Biotechnology, 34 (2016) 810–811.

[62]. Cao C, Ying Y-L, Hu Z-L, Liao D-F, Tian H, Long Y-T, Discrimination of oligonucleotides of different lengths with a wild-type aerolysin nanopore, Nature Nanotech., (2016) 713–718.

[63]. Cao C, Yu J, Wang Y-Q, Ying Y-L, Long Y-T, Driven Translocation of Polynucleotides Through an Aerolysin Nanopore, Analytical Chemistry, (2016) 5046–5049. [PubMed: 27120503]

[64]. Li J, Stein D, McMullan C, Branton D, Aziz MJ, Golovchenko JA, Ion-beam sculpting at nanometre length scales, Nature, 412 (2001) 166–169. [PubMed: 11449268]

[65]. Storm AJ, Chen JH, Ling XS, Zandbergen HW, Dekker C, Fabrication of solid-state nanopores with single-nanometre precision, Nature Materials, 2 (2003) 537–540. [PubMed: 12858166]

[66]. Kwok H, Briggs K, Tabard-Cossa V, Nanopore fabrication by controlled dielectric breakdown, PLoS ONE, e92880 (2014). [PubMed: 24658537]

[67]. Rollings RC, Kuan AT, Golovchenko JA, Ion selectivity of graphene nanopores, Nature Communications, 7 (2016) 11408.

[68]. Heerema SJ, Vicarelli L, Pud S, Schouten RN, Zandbergen HW, Dekker C, Probing DNA translocations with inplane current signals in a graphene nanoribbon with a nanopore, ACS Nano, (2018) 2623–2633. [PubMed: 29474060]

[69]. Feng J, Liu K, Bulushev RD, Khlybov S, Dumcenco D, Kis A, Radenovic A, Identification of single nucleotides in MoS2 nanopores, Nature Nanotechnology, 10 (2015) 1070–1076.

[70]. Gilbert SM, Dunn G, Azizi A, Pham T, Shevitski B, Dimitrov E, Liu S, Aloni S, Zettl A, Fabrication of subnanometer-precision nanopores in hexagonal boron nitride, Scientific Reports, 7 (2017) 4–8. [PubMed: 28127054]

[71]. Danda G, Masih Das P, Chou YC, Mlack JT, Parkin WM, Naylor CH, Fujisawa K, Zhang T, Fulton LB, Terrones M, Johnson ATC, Drndić M, Monolayer WS2 nanopores for DNA translocation with light-adjustable sizes, ACS Nano, 11 (2017) 1937–1945. [PubMed: 28125779]

[72]. Rodríguez-Manzo JA, Puster M, Nicolaï A, Meunier V, Drndic M, DNA Translocation in Nanometer Thick Silicon Nanopores, ACS Nano, 9 (2015) 6555–6564. [PubMed: 26035079]

[73]. Fuller CW, Kumar S, Porel M, Chien M, Bibillo A, Stranges PB, Dorwart M, Tao C, Li Z, Guo W, Shi S, Korenblum D, Trans A, Aguirre A, Liu E, Harada ET, Pollard J, Bhat A, Cech C, Yang A, Arnold C, Palla M, Hovis J, Chen R, Morozova I, Kalachikov S, Russo JJ, Kasianowicz JJ, Davis R, Roever S, Church GM, Ju J, Real-time single-molecule electronic DNA sequencing by synthesis using polymer-tagged nucleotides on a nanopore array, Proc. Natl. Acad. Sci. U S A, 113 (2016) 5233–5238. [PubMed: 27091962]

[74]. Torre R, Larkin J, Singer A, Meller A, Fabrication and characterization of solid-state nanopore arrays for high throughput DNA sequencing, Nanotech., 23 (2013) 385308.

[75]. Tropini C, Marziali A, Multi-nanopore force spectroscopy for DNA analysis, Biophys. J, 92 (2007) 1632–1637. [PubMed: 17158571]

[76]. Cadinu P, Campolo G, Pud S, Yang W, Edel JB, Dekker C, Ivanov AP, Double Barrel Nanopores as a New Tool for Controlling Single-Molecule Transport, Nano Letters, 18 (2018) 2738–2745. [PubMed: 29569930]

[77]. Cadinu P, Paulose Nadappuram B, Lee D, Sze JYY, Campolo G, Zhang Y, Shevchuk A, Ladame S, Albrecht T, Korchev YE, Ivanov AP, Edel JB, Single molecule trapping and sensing using dual nanopores separated by a zeptolitre nanobridge, Nano Letters, 17 (2017) 6376–6384. [PubMed: 28862004]

[78]. Gornall JL, Mahendran KR, Pambos OJ, Steinbock LJ, Otto O, Chimerel C, Winterhalter M, Keyser UF, Simple reconstitution of protein pores in nano lipid bilayers, Nano Letters, 11 (2011) 3334–3340. [PubMed: 21749149]

[79]. Balan A, Chien C-C, Engelke R, Drndic M, Suspended solid-state membranes on glass chips with sub 1-pF capacitance for biomolecule sensing applications, Scientific Reports, 5 (2015) 2458.

[80]. Balan A, Machielse B, Niedzwiecki D, Lin J, Ong P, Engelke R, Shepard KL, Drndić M, Improving signal-to-noise performance for DNA translocation in solid-state nanopores at MHz bandwidths, Nano Letters, 14 (2014) 7215–7220. [PubMed: 25418589]

[81]. Arcadia CE, Reyes CC, Rosenstein JK, In-situ nanopore fabrication and single-molecule sensing with microscale liquid contacts, ACS Nano, 11 (2017) 4907–4915. [PubMed: 28485922]

[82]. Ferrari G, Farina M, Guagliardo F, Carminati M, Sampietro M, Ultra-low-noise CMOS current preamplifier from DC to 1 MHz, Electronics Letters, 45 (2009) 1278–1280.

[83]. Ferrari G, Sampietro M, Wide bandwidth transimpedance amplifier for extremely high sensitivity continuous measurements, Rev. Sci. Instruments 78 (2007).

[84]. Crescentini M, Bennati M, Carminati M, Tartagni M, Noise limits of CMOS current interfaces for biosensors: A review, IEEE Transactions on Biomedical Circuits and Systems, 8 (2014) 278–292. [PubMed: 24875287]

[85]. Garalde DR, Snell EA, Jachimowicz D, Sipos B, Lloyd JH, Bruce M, Pantic N, Admassu T, James P, Warland A, Jordan M, Ciccone J, Serra S, Keenan J, Martin S, McNeill L, Wallace EJ, Jayasinghe L, Wright C, Blasco J, Young S, Brocklebank D, Juul S, Clarke J, Heron AJ, Turner DJ, Highly parallel direct RNA sequencing on an array of nanopores, Nature Methods, 15 (2018) 201–206. [PubMed: 29334379]

[86]. Cherf GM, Lieberman KR, Rashid H, Lam CE, Karplus K, Akeson M, Automated forward and reverse ratcheting of DNA in a nanopore at 5-Å precision, Nature biotechnology, 30 (2012) 344–348.

[87]. He Y, Tsutsui M, Scheicher RH, Bai F, Taniguchi M, Kawai T, Thermophoretic manipulation of DNA translocation through nanopores, ACS Nano, 7 (2013) 538–546. [PubMed: 23199225]

[88]. Wanunu M, Morrison W, Rabin Y, Grosberg AY, Meller A, Electrostatic focusing of unlabelled DNA into nanoscale pores using a salt gradient, Nature Nanotechnology, 5 (2010) 160–165.

[89]. Valiyaveetil FI, Leonetti M, Muir TW, MacKinnon R, Ion selectivity in a semisynthetic K+ channel locked in the conductive conformation, Science (New York, NY), 314 (2006) 1004–1007.

[90]. MacKinnon R, New insights into the structure and function of potassium channels, Current Opin. Neurobiol, 1 (1991) 14–19.

[91]. Liu X, Betzenhauser MJ, Reiken S, Meli AC, Xie W, Chen B-X, Arancio O, Marks AR, Role of leaky neuronal ryanodine receptors in stress-induced cognitive dysfunction, Cell, 150 (2012) 1055–1067. [PubMed: 22939628]

[92]. Andersson DC, Betzenhauser MJ, Reiken S, Meli AC, Umanskaya A, Xie W, Shiomi T, Zalk R, Lacampagne A, Marks AR, Ryanodine receptor oxidation causes intracellular calcium leak and muscle weakness in aging, Cell Metabolism, 14 (2011) 196–207. [PubMed: 21803290]

[93]. Neher E, Sakmann B, Single-channel currents recorded from membrane of denervated frog muscle fibres, Nature, 260 (1976) 799–802. [PubMed: 1083489]

[94]. Conti F, Neher E, Single channel recordings of K+ currents in squid axons, Nature, 285 (1980) 140–143. [PubMed: 6246440]

[95]. Katz B, Miledi R, The statistical nature of the acetylcholine potential and its molecular components, J. Physiol, 321 (1972) 665–699.

[96]. Sakmann B, Neher E, Patch Clamp Techniques for Studying Ionic Channels in Excitable Membranes, Annual review of physiology, 46 (1984) 455–472.

[97]. Sakmann B, Patlak J, Neher E, Single acetylcholine-activated channels show burst-kinetics in presence of desensitizing concentrations of agonist, Nature, 286 (1980) 71–73. [PubMed: 6248795]

[98]. Hamill OP, Marty A, Neher E, Sakmann B, Sigworth FJ, Improved patch-clamp techniques for high-resolution current recording from cells and cell-Free membrane patches, J. Physiol, 391 (1981) 85–100.

[99]. Mortensen M, Smart TG, Single-channel recording of ligand-gated ion channels, Nature Protocols, 2 (2007) 2826–2841. [PubMed: 18007618]

[100]. Zhang B, Galusha J, Shiozawa PG, Wang G, Bergren AJ, Jones RM, White RJ, Ervin EN, Cauley CC, White HS, Bench-top method for fabricating glass-sealed nanodisk electrodes, glass nanopore electrodes, and glass nanopore membranes of controlled size, Anal. Chem , 79 (2007) 4778–4787. [PubMed: 17550232]

[101]. White RJ, Ervin EN, Yang T, Chen X, Daniel S, Cremer PS, White HS, Single ion-channel recordings using glass nanopore membranes, J. Am. Chem. Soc, 129 (2007) 11766–11775. [PubMed: 17784758]

[102]. Klemic KG, Klemic JF, Reed MA, Sigworth FJ, Micromolded PDMS planar electrode allows patch clamp electrical recordings from cells., Biosensors and Bioelectronics, 17 (2002) 597–604. [PubMed: 11959483]

[103]. Weerakoon P, Culurciello E, Yang Y, Santos-Sacchi J, Kindlmann PJ, Sigworth FJ, Patch-clamp amplifiers on a chip, J. Neuroscience Meth, 192 (2010) 187–192.

[104]. Niles WD, Levis RA, Cohen FS, Planar bilayer membranes made from phospholipid monolayers form by a thinning process, Biophys. J, 53 (1988) 327–335. [PubMed: 3349129]

[105]. Gentet LJ, Stuart GJ, Clements JD, Direct measurement of specific membrane capacitance in neurons, Biophys. J, 79 (2000) 314–320. [PubMed: 10866957]

[106]. Montal M, Mueller P, Formation of bimolecular membranes from lipid monolayers and a study of their electrical properties, Proc. Natl. Acad. Sci. U S A, 69 (1972) 3561–3566. [PubMed: 4509315]

[107]. Mueller P, Rudin DO, Tien HT, Wescott WC, Reconstitution of cell membrane structure in vitro and its transformation into an excitable system, Nature, 194 (1962) 979–980. [PubMed: 14476933]

[108]. Braun CJ, Baer T, Moroni A, Thiel G, Pseudo painting/air bubble technique for planar lipid bilayers, J. Neuroscience Meth, 233 (2014) 13–17.

[109]. Zakharian E, Recording of ion channel activity in planar lipid bilayer experiments, Methods Mol. Biol, 998 (2013) 109–118. [PubMed: 23529424]

[110]. Bartsch P, Walter C, Selenschik P, Honigmann A, Wagner R, Horizontal bilayer for electrical and optical recordings, Materials, 5 (2012) 2705–2730.

[111]. Braun CJ, Lachnit C, Becker P, Henkes LM, Arrigoni C, Kast SM, Moroni A, Thiel G, Schroeder I, Viral potassium channels as a robust model system for studies of membrane–protein interaction, BBA-Biomem., 1838 (2013) 1096–1103.

[112]. Winterstein L-M, Kukovetz K, Rauh O, Turman DL, Braun C, Moroni A, Schroeder I, Thiel G, Reconstitution and functional characterization of ion channels from nanodiscs in lipid bilayers, The Journal of general physiology, (2018) jgp.201711904.

[113]. Hanke W, Incorporation of ion channels by fusion, in: Miller C (Ed.) Ion channel reconstitution Springer US, Boston, MA, 1986, pp. 141–153.

[114]. Pantoja R, Sigg D, Blunck R, Benzanilla F, Heath JR, Bilayer reconstitution of voltage-dependent ion channels using a microfabricated silicon chip, Biophys. J, 81 (2001) 2389–2394. [PubMed: 11566808]

[115]. Cohen FS, Niles WD, Akabas MH, Fusion of phospholipid vesicles with a planar membrane depends on the membrane permeability of the solute used to create the osmotic pressure, J. Gen. Phys, 93 (1989) 201–210.

[116]. Cohen FS, Fusion of phospholipid vesicles with planar phospholipid bilayer membranes. II. Incorporation of a vesicular membrane marker into the planar membrane, J. Gen. Phys, 75 (1980) 251–270.

[117]. Miller C, Arvan P, Telford JN, Racker E, Ca++-induced fusion of proteoliposomes: Dependence on transmembrane osmotic gradient, J. Mem. Biol, 30 (1976) 271–282.

[118]. Niles WD, Cohen FS, Video fluorescence microscopy studies of phospholipid vesicle fusion with a planar phospholipid membrane. Nature of membrane-membrane interactions and detection of release of contents, J. Gen. Phys, 90 (1987) 703–735.

[119]. Woodbury DJ, Miller C, Nystatin-induced liposome fusion. A versatile approach to ion channel reconstitution into planar bilayers, Biophys. J, 58 (1990) 833–839. [PubMed: 1701101]

[120]. Zagnoni M, Sandison ME, Marius P, Lee AG, Morgan H, Controlled delivery of proteins into bilayer lipid membranes on chip, Lab on a Chip, 7 (2007) 1176–1183. [PubMed: 17713617]

[121]. Schroeder I, Thiel G, Hansen U-P, Ca2+ block and flickering both contribute to the negative slope of the IV curve in BK channels, J. Gen. Phys, 141 (2013) 499–505.

[122]. Schroeder I, Hansen U-P, Saturation and microsecond gating of current indicate depletion-induced instability of the MaxiK selectivity filter, J. Gen. Phys, 130 (2007) 83–97.

[123]. Mukherjee S, Thomas NL, Williams AJ, A mechanistic description of gating of the human cardiac ryanodine receptor in a regulated minimal environment, J. Gen. Phys, 140 (2012)139–158.

[124]. Rauh O, Hansen U-P, Mach S, Hartel AJW, Shepard KL, Thiel G, Schroeder I, Extended beta distributions open the access to fast gating in bilayer experiments-assigning the voltage-dependent gating to the selectivity filter, FEBS let, 69 (2017) 3561.

[125]. Last NB, Sun S, Pham MC, Miller C, Molecular determinants of permeation in a fluoride-specific ion channel, eLIFE, (2017).

[126]. Last NB, Kolmakova-Partensky L, Shane T, Miller C, Mechanistic signs of double-barreled structure in a fluoride ion channel, eLIFE, (2016).

[127]. Gutsmann T, Heimburg T, Keyser U, Mahendran KR, Winterhalter M, Protein reconstitution into freestanding planar lipid membranes for electrophysiological characterization, Nature Protocols, 10 (2014) 188–198. [PubMed: 25551663]

[128]. Wonderlin WF, Finkel A, French RJ, Optimizing planar lipid bilayer single-channel recordings for high resolution with rapid voltage steps, Biophys. J, 58 (1990) 289–297. [PubMed: 1698470]

[129]. L Brown A, E Johnson B, B Goodman M, Making patch-pipettes and sharp electrodes with a programmable puller, JOVE, 8 (2008) pii 939.

[130]. Iwamoto M, Oiki S, Contact bubble bilayers with flush drainage, Scientific Reports, 5 (2015) 979.

[131]. Hanke W, Methfessel C, Wilmsen U, Boheim G, Ion channel reconstitution into lipid bilayer membranes on glass patch pipettes, Bioelectrochem and Bioenerget., 12 (1984) 329–339.

[132]. Coronado R, Latorre R, Phospholipid bilayers made from monolayers on patch-clamp pipettes, Biophys. J, 43 (1983) 231–236. [PubMed: 6193818]

[133]. Petrov AG, Flexoelectricity of model and living membranes, BBA-Biomem., 1561 (2001) 1–25.

[134]. Heimburg T, Lipid ion channels, Biophys. Chem, 150 (2010) 2–22. [PubMed: 20385440]

[135]. Miller C, White MM, A voltage-dependent chloride conductance channel from torpedo electrolax membrane Ann. N.Y. Acad. Sci, 341 (1980) 534–551.

[136]. Weerakoon P, Culurciello E, Klemic KG, Sigworth FJ, An integrated patch-clamp potentiostat with electrode compensation, IEEE Trans. on Biomed. Circuits and Sys, 3 (2009) 117–125.

[137]. Simon A, Girard-Egrot AP, Sauter F, Pudda C, Picollet-D'Hahan N, Blum L, Chatelain FC, Fuchs A, Formation and stability of a suspended biomimetic lipid bilayer on silicon submicrometer-sized pores, J. Colloid and Interface Sci, 308 (2007) 337–343. [PubMed: 17275017]

[138]. Urisu T, Rahman MM, Uno H, Tero R, Nonogaki Y, Formation of high-resistance supported lipid bilayer on the surface of a silicon substrate with microelectrodes, Nanomed. Nanotech. Biol. Med, 1 (2005) 317–322.

[139]. Tadaki D, Yamaura D, Araki S, Yoshida M, Arata K, Ohori T, Ishibashi K.-i., Kato M, Ma T, Miyata R, Tozawa Y, Yamamoto H, Niwano M, Hirano-Iwata A, Mechanically stable solvent-free lipid bilayers in nano- and micro-tapered apertures for reconstitution of cell-free synthesized hERG channels, Scientific Reports, 7 (2017) 253. [PubMed: 28325925]

[140]. Clarke OB, Hendrickson WA, Structures of the colossal RyR1 calcium release channel, Curr. Opin. Struct. Biol , 39 (2016) 144–152. [PubMed: 27687475]

[141]. Bezprozvanny l., Watras J, Ehrlich BE, Bell-shaped calcium-response curves of lns(l,4,5)P3- and calcium-gated channels from endoplasmic reticulum of cerebellum, Nature, 351 (1991) 751–754. [PubMed: 1648178]

[142]. Colquhoun D, Sigworth FJ, Fitting and statistical analysis of single-channel records, in: Sakmann B, Neher E (Eds.) Single-Channel Recording, Springer US, Boston, MA, 1995, pp. 483–587.

[143]. Hansen U-P, Albertsen A, Moldaenke C, Draber S, Detecting events in signals from sensors: the Hinkley detector is the answer, Sensors and Materials, 7 (1995) 289–300.

[144]. Schultze R, Draber S, A nonlinear filter algorithm for the detection of jumps in patch-clamp data, J. Mem. Biol, 132 (1993) 41–52.

[145]. Draber S, Schultze R, Detection of jumps in single-channel data containing subconductance levels, Biophys. J, 67 (1994) 1404–1413. [PubMed: 7529580]

[146]. Pein F, Tecuapetla-Gómez I, Schutte OM, Steinem C, Munk A, Fully automatic multiresolution idealization for filtered ion channel recordings: flickering event detection, IEEE Trans. Nanobiosci, 17 (2018) 300–320.

[147]. Ball FG, Rice JA, Stochastic models for ion channels: Introduction and bibliography, Math. Biosci, 112 (1992) 189–206. [PubMed: 1283350]

[148]. Blatz AL, Magleby KL, Correcting single channel data for missed events, Biopyhs. J, 49 (1986) 967–980.

[149]. Feng Qin LL, Model-based fitting of single-channel dwell-time distributions, Biophys. J, 87 (2004) 1657–1671. [PubMed: 15345545]

[150]. Colquhoun D, Hatton CJ, Hawkes AG, The quality of maximum likelihood estimates of ion channel rate constants, J. Physiol, 547 (2003) 699–728. [PubMed: 12562901]

[151]. Crouzy S, Sigworth FJ, Yet another approach to the dwell-time omission problem of single-channel analysis, Biopyhs. J, 58 (1990) 731–743.

[152]. Horn R, Statistical properties of single sodium channels, J. Gen. Phys, 84 (1984) 505–534.

[153]. Fredkin DR, Rice JA, Fast evaluation of the likelihood of an HMM: ion channel currents with filtering and colored noise, IEEE Trans. Signal Process, 49 (2001) 625–633.

[154]. Albertsen A, Hansen U-P, Estimation of kinetic rate constants from multi-channel recordings by a direct fit of the time series, Biophys. J, 67 (1994) 1393–1403. [PubMed: 7529579]

[155]. Farokhi A, Keunecke M, Hansen U-P, The anomalous mole fraction effect in chara: gating at the edge of temporal resolution, Biophys. J, 79 (2000) 3072–3082. [PubMed: 11106613]

[156]. Heinemann SH, Sigworth FJ, Open channel noise. IV. Estimation of rapid kinetics of formamide block in gramicidin A channels, Biophys. J, 54 (1988) 757–764. [PubMed: 2465033]

[157]. Schroeder I, How to resolve microsecond current fluctuations in single ion channels: The power of beta distributions, Channels, 9 (2015) 262–280. [PubMed: 26368656]

[158]. Hille B, Ion Channels of Excitable Membranes, 3rd ed., Sinauer Associates Inc. Sunderland 2001.

[159]. Fitzhugh R, Statistical properties of the asymmetric random telegraph signal, with applications to single-channel analysis, Math. Biosci, 64 (1982) 75–89.

[160]. Yellen G, Ionic permeation and blockade in Ca2+-activated K+ channels of bovine chromaffin cells, J. Gen. Phys, 84 (1984) 157–186.

[161]. Weise R, Gradmann D, K+ channel in the tonoplast of Chara: decrease of conductance by blocks in 100 nanosecond range and induction of oligo-or poly-subconductance gating modes, J. Mem. Biol, (2000) 87–93.

[162]. Bertl A, Slayman C, Gradmann D, Gating and conductance in an outward-rectifying K+ channel from the plasma membrane of Saccharomyces cerevisiae, J. Mem. Biol, 132 (1993)183–199.

[163]. Klieber HG, Gradmann D, Enzyme kinetics of the prime K+ channel in the tonoplast of Chara: selectivity and inhibition, J. Mem. Biol, 132 (1993) 253–265.

[164]. Tsushima RG, Kelly JE, Wasserstrom JA, Characteristics of cocaine block of purified cardiac sarcoplasmic reticulum calcium release channels, Biopyhs. J, 70 (1996) 1263–1274.

[165]. Heinemann SH, Sigworth FJ, Open channel noise. VI. Analysis of amplitude histograms to determine rapid kinetic parameters, Biophys. J, 60 (1991) 577–587. [PubMed: 1718467]

[166]. Riessner T, Level detection and extended beta distributions for the analysis of fast rate constants of Markov processes in sampled data, Shaker Verlag Aachen 1998.

[167]. Riessner T, Hansen U-P, Fast switching in patch clamp records as analyzed by an extended theory of multi-channel beta distributions, 10th International Workshop on Plant Membrane Biology Regensburg 1996.

[168]. White PJ, Ridout MS, The estimation of rapid rate constants from current-amplitude frequency distributions of single-channel recordings, J. Mem. Biol, (1998) 115–129.

[169]. Schroeder I, Hansen U-P, Strengths and limits of Beta distributions as a means of reconstructing the true single-channel current in patch clamp time series with fast gating, J. Mem. Biol, 210 (2006) 199–212.

[170]. Schroeder I, Harlfinger P, Huth T, Hansen U-P, A subsequent fit of time series and amplitude histogram of patch-clamp records reveals rate constants up to 1 per microsecond, J. Mem. Biol, (2005) 83–99.

[171]. Baum LE, Petrie T, Statistical inference for probabilistic functions of finite state markov chains, Annals Math. Stats, 37 (1966) 1554–1563.

[172]. Schroeder I, Hansen U-P, Interference of shot noise of open-channel current with analysis of fast gating: patchers do not (yet) have to care, J. Mem. Biol, 229 (2009) 153–163.

[173]. Rauh O, Urban M, Henkes LM, Winterstein T, Greiner T, Van Etten JL, Moroni A, Kast SM, Thiel G, Schroeder I, Identification of intrahelical bifurcated H-bonds as a new type of gate in K(+) channels, J. Am. Chem. Soc, 139 (2017) 7494–7503. [PubMed: 28499087]

[174]. Brauser A, Schroeder I, Gutsmann T, Cosentino C, Moroni A, Hansen U-P, Winterhalter M, Modulation of enrofloxacin binding in OmpF by Mg2+ as revealed by the analysis of fast flickering single-porin current, J. Gen. Phys, 140 (2012) 69–82.

[175]. Abenavoli A, DiFrancesco ML, Schroeder I, Epimashko S, Gazzarrini S, Hansen U-P, Thiel G, Moroni A, Fast and slow gating are inherent properties of the pore module of the K+ channel Kcv, J. Gen. Phys, 134 (2009) 219–229.

[176]. Rauh O, Hansen U-P, Scheub DD, Thiel G, Schroeder I, Site-specific ion occupation in the selectivity filter causes voltage-dependent gating in a viral K+ channel, Scientific Reports, 8 (2018) 10406. [PubMed: 29991721]

[177]. Domene C, Grottesi A, Sansom MSP, Filter flexibility and distortion in a bacterial inward rectifier K+ channel: simulation studies of KirBac1.1, Biophys. J, 87 (2004) 256–267. [PubMed: 15240462]

[178]. Crozier PS, Henderson D, Rowley RL, Busath DD, Model channel ion currents in NaCl–SPC/E solution with applied–field molecular dynamics, Biophys. J, 81 (2001) 3077–3089. [PubMed: 11720976]

[179]. Jensen MØ, Jogini V, Eastwood MP, Shaw DE, Atomic-level simulation of current–voltage relationships in single-file ion channels, J. Gen. Phys, 141 (2013) 619.

[180]. Lanner JT, Georgiou DK, Joshi AD, Hamilton SL, Ryanodine Receptors: structure, expression, molecular details, and function in calcium release, Cold Spring Harbor Pers. in Biol, 2 (2010).

[181]. Smeazzetto S, Schröder I, Thiel G, Moncelli MR, Phospholamban generates cation selective ion channels, Phys. Chem. Chem. Phys, 13 (2011) 12935–12939. [PubMed: 21687864]

[182]. Tayefeh S, Kloss T, Thiel G, Hertel B, Moroni A, Kast SM, Molecular dynamics simulation of the cytosolic mouth in Kcv-type potassium channels, Biochemistry, 46 (2007) 4826–4839. [PubMed: 17397187]

- Study of ion channels and solid-state nanopores are bandwidth-limited to 10–100 kHz.
- Signal to noise ratio is dominated by parasitic capacitance.
- Discussion of limitations of electronics and demonstration of solutions to limitations.
- Integration of electronics and lipid-bilayer or solid-state nanopores allows bandwidth up to 10 MHz.
- High bandwidth allows detection of dynamics in-accessible with conventional methods.

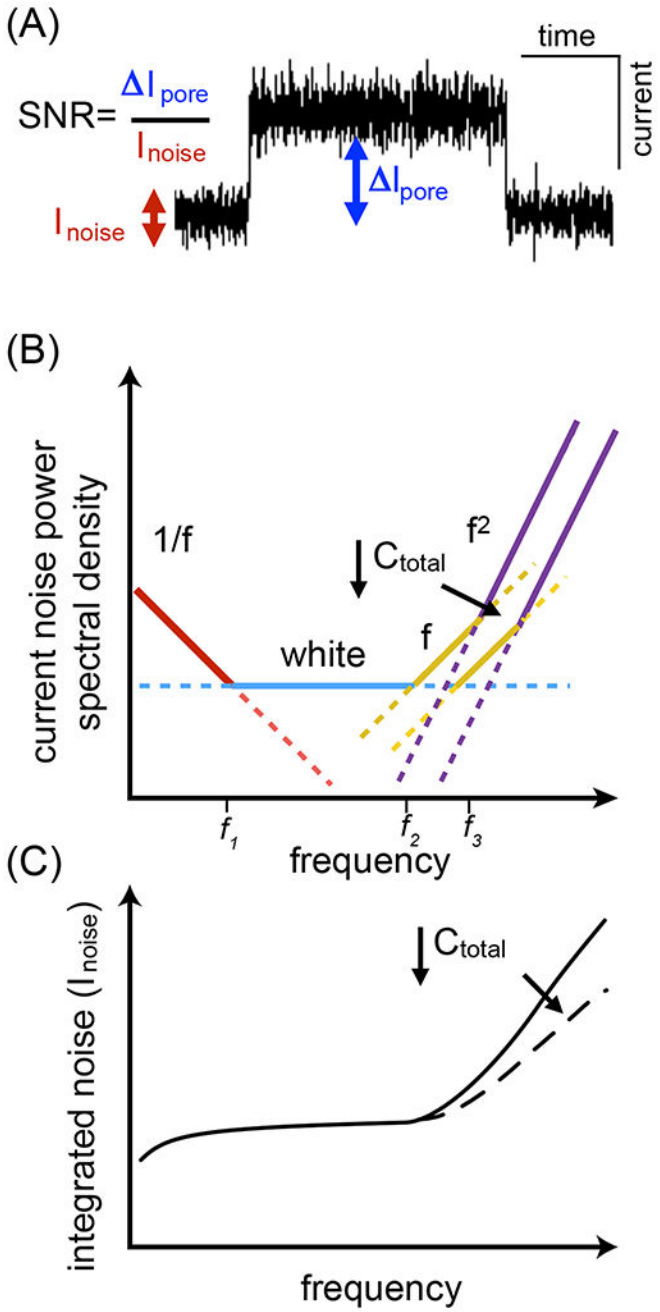

Figure 1. Noise considerations limiting high bandwidth recordings.

(A) Signal-to-noise ratio defined as the current through the pore I_{pore} divided by the current noise I_{noise} of the measurement system. **(B)** Qualitative plot of the current noise power spectral density for the different noise contributors on a log log scale. 1/f-noise at low frequencies (red line). Spectrum reaches a corner and becomes determined by frequency independent white noise (blue line). Another corner is reached and the spectrum increases linearly with frequency, f-noise (orange line). At high frequencies the spectrum scales as f^2 (purple line). The appearance of f and f^2 noise can be pushed to higher frequencies by

lowering C_{total}. **(C)** Qualitative plot of the integrated noise spectrum, equivalent to I_{noise}, on a log log plot. Dashed line represents the effect of lowering I_{noise} by reducing C_{total}.

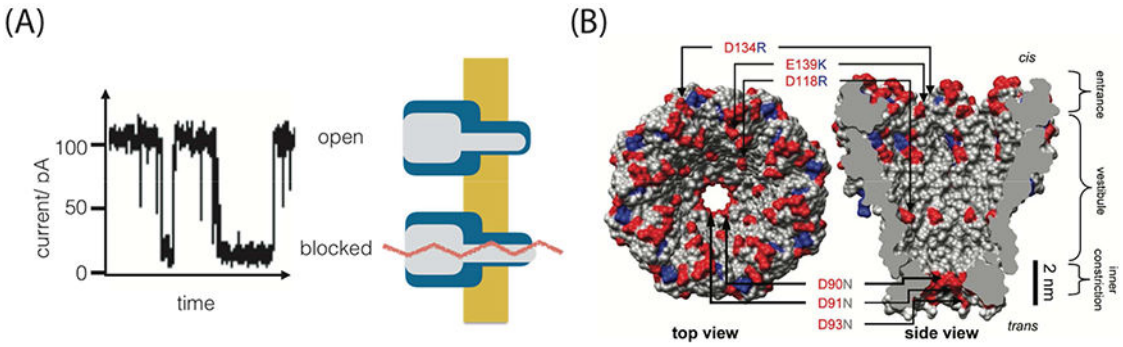

Figure 2. Stochastic sensing with biological nanopores.

(A) Typical current recording with a nanopore. The current is high when the pore is not obstructed and low when the pore is blocked by a molecule e.g. DNA (Altered by permission from Springer Nature: Nature Biotechnology, The potential challenges of nanopore sequencing, D. Branton et al., Copyright 2008 Sprinter Nature, 2008). **(B)** In addition to the most frequently used α-hemolysin also other pores like MspA, a porin from the bacterium *Mycobacterium smegmatis* is used. These systems benefit from the well known structure of these pores and the possibility of their genetic manipulation. (Altered by permission from National academy of science: PNAS, Single-molecule DNA detection with an engineered MspA protein pore, T. Butler et al., Copyright 2008 National Academy of Science, 2008).

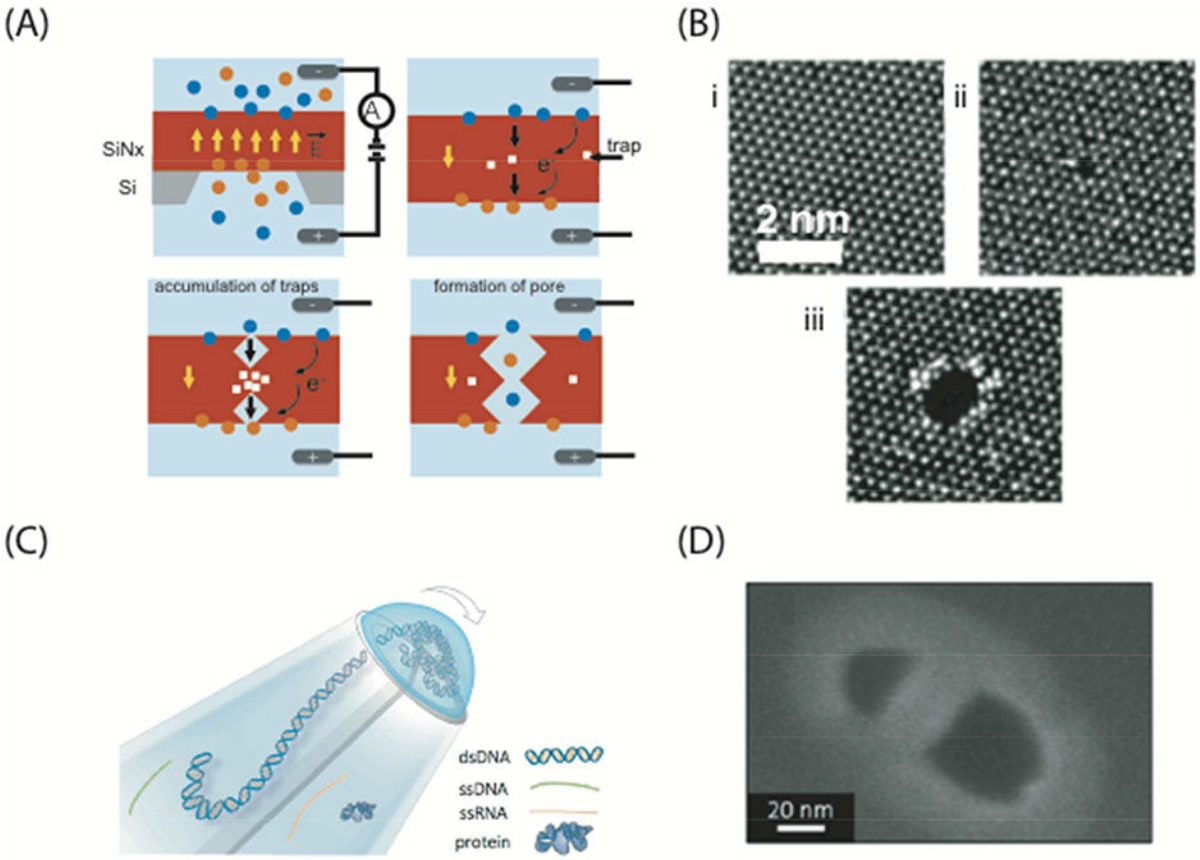

Figure 3. Solid-state nanopores.

(A) Controlled dielectric breakdown for nanopore formation (Figure redrawn from [66]). **(B)** Atomically thin nanopores created using 2-D materialsWS_2 (Adapted with permission from American Chemical Society: ACS Nano, Monolayer WS_2 nanopores for DNA translocation with light-adjustable size, G. Danda et al., Copyright 2017 American Chemical Society, 2017). **(C)** Schematic drawing and **(D)** electron micrograph of double barreled glass nanopipettes with openings of diameters of a few 10's of nm to trap molecules for arbitrarily long periods of time (Adapted with permission from American Chemical Society: Nano Letters, Double barrel nanopores as a new tool for controlling single-molecule transport, P. Cadinu et al., CC-BY License, Copyright 2018 American Chemical Society, 2018).

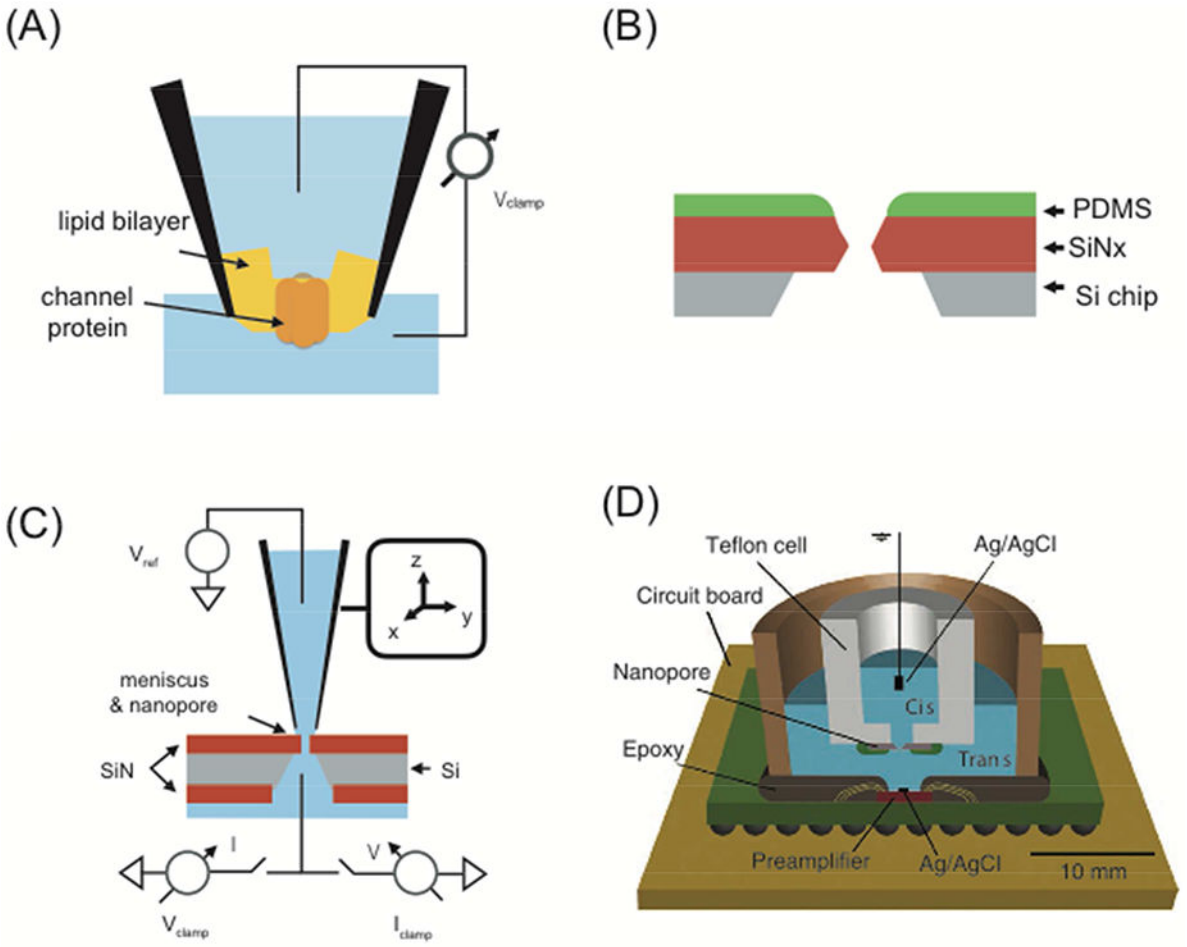

Figure 4. Low-capacitance techniques for nanopore recordings.

(A) A common technique for reducing membrane capacitance in biological nanopore recordings is by forming a suspended bilayer at the tip of a patch pipette or nanopipette (Adapted with permission from American Chemical Society: Nanoletters, Double barrel nanopores as a new tool for controlling single-molecule transport, JL Gornall et al., Copyright 2011 American Chemical Society, 2011). **(B)** For solid-state nanopores, the membrane can be passivated by using e.g. PDMS (redrawn from [7]). **(C)** With solid-state nanopores, the effective contact area can be reduced to μm sized droplet by using a pipette mounted on a manipulator, resulting in extremely low capacitances (Adapted with permission from American Chemical Society: ACS Nano, In situ nanopores fabrication and single-molecule sensing with microscale liquid contacts, C Arcadia et al., Copyright 2017 American Chemical Society, 2017) **(D)** Tight integration of fluidics directly on top of custom-designed amplifiers can be used to significantly reduce wiring capacitance. (Adapted with permission from Springer Nature: Nature Methods, Integrated nanopores sensing platform with sub-microsecond temporal resolution, J Rosenstein et al., Copyright 2012 Springer Nature , 2012).

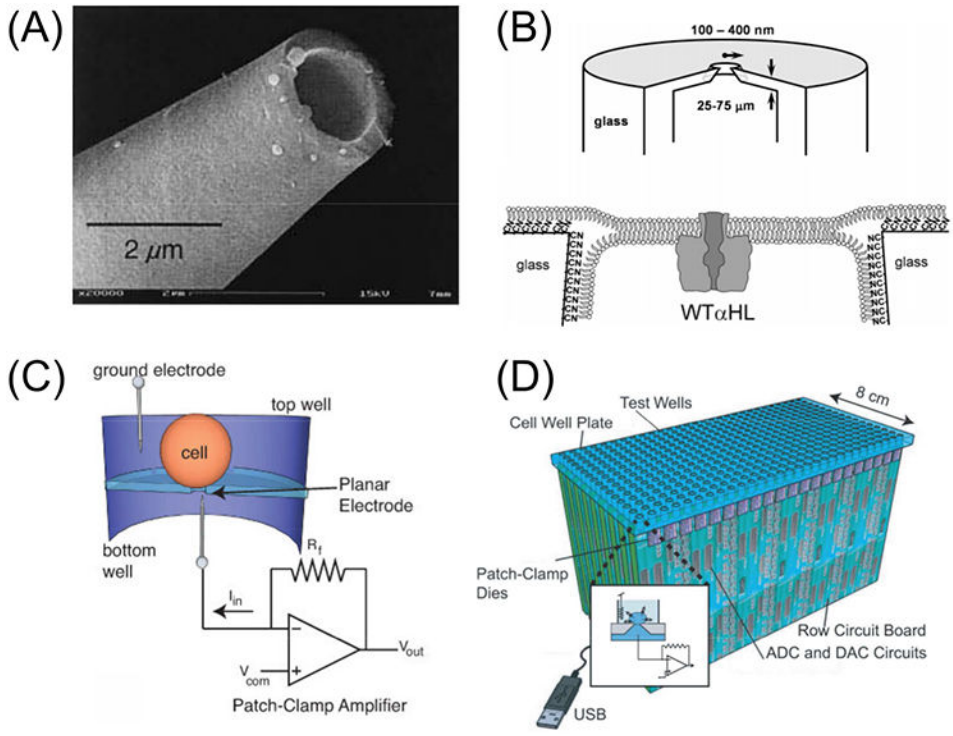

Figure 5. Approaches in single-cell and single-channel recordings.

(A) SEM image of patch pipette (Adapted with permission from Elsevier: Biophysical Journal, Whole cell patch clamp recordings performed on a planar glass chip, N. Fertig et al., Copyright 2002 Elsevier, 2002). **(B)** Approaches for reducing total capacitance in the measurement system: micro-fabricated glass nanopores lower effective membranes area and hence reduce C_{mem} in single channel recordings (Adapted with permission from American Chemical Society: Journal of American Chemical Society, Single ion-channel recordings using glass nanopores membranes, R White et al., Copyright 2007 American Chemical Society, 2007). **(C)** and **(D)** Integrated approaches using arrays of amplifiers for parallel recordings of cells (Figure reprint with permission from IEEE: Biomedical Circuits and Systems, Transactions on IEEE, An integrated patch-clamp potentiostat with electrode compensation, P. Weerakoon et al., Copyright 2009 IEEE, 2009).

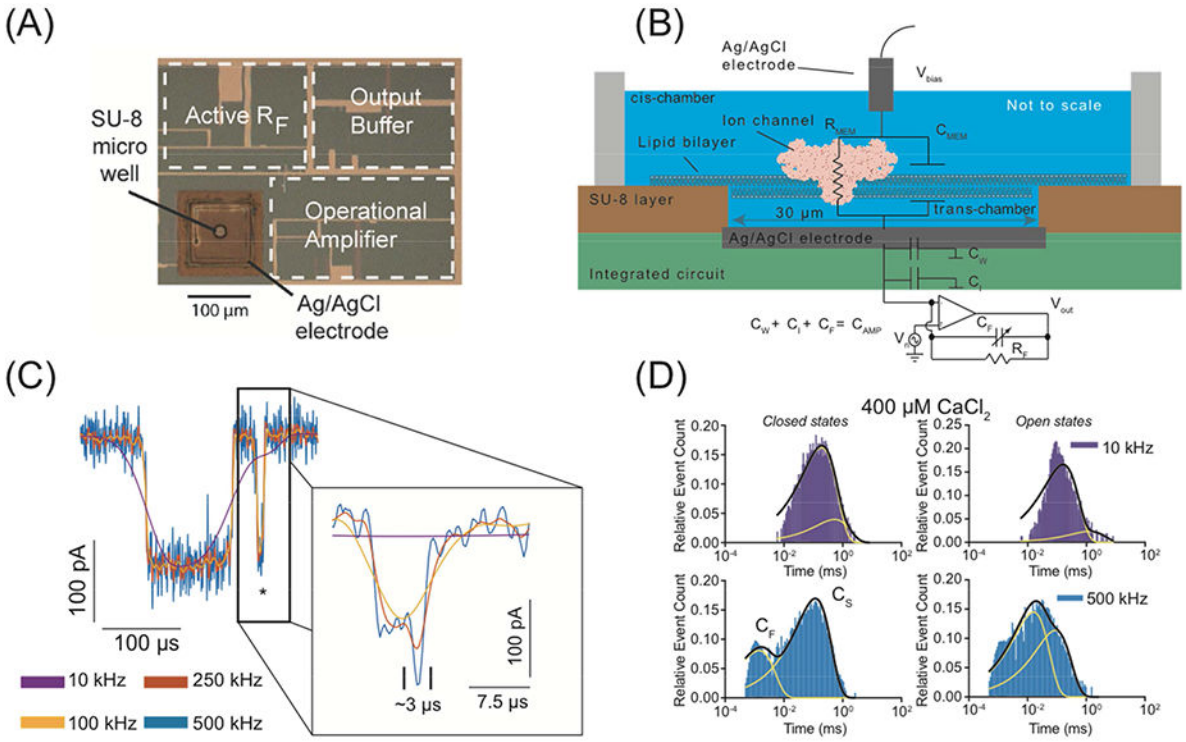

Figure 6. Single-channel recordings in black lipid membranes on a CMOS platform.

(A) Picture of a CMOS-integrated patch-clamp amplifier (Reprint with permission from American Chemical Society: Nano Letters, Single ion channel recordings with CMOS-anchored lipid membranes, J Rosenstein et al., Copyright 2013 American Chemical Society, 2013). **(B)** Schematics of CMOS-supported lipid bilayer for high-bandwidth recordings. **(C)** Exemplary channel fluctuations of the type 1 ryanodine receptor at different bandwidth: 10 (purple), 100 (yellow), 250 (orange) and 500 (blue) kHz. **(D)** Dwell-time histograms of open and closed state of recordings of the ryanodine type 1 receptor at 10 (purple) and 500 kHz (blue) in the presence of 400 µM free Calcium. (Adapted with permission from National Academy of Science: PNAS, Single-channel recordings of RyR1 at microsecond resolution in CMOS-suspended membranes, A Hartel et al., Copyright 2018 National Academy of Science, 2018)

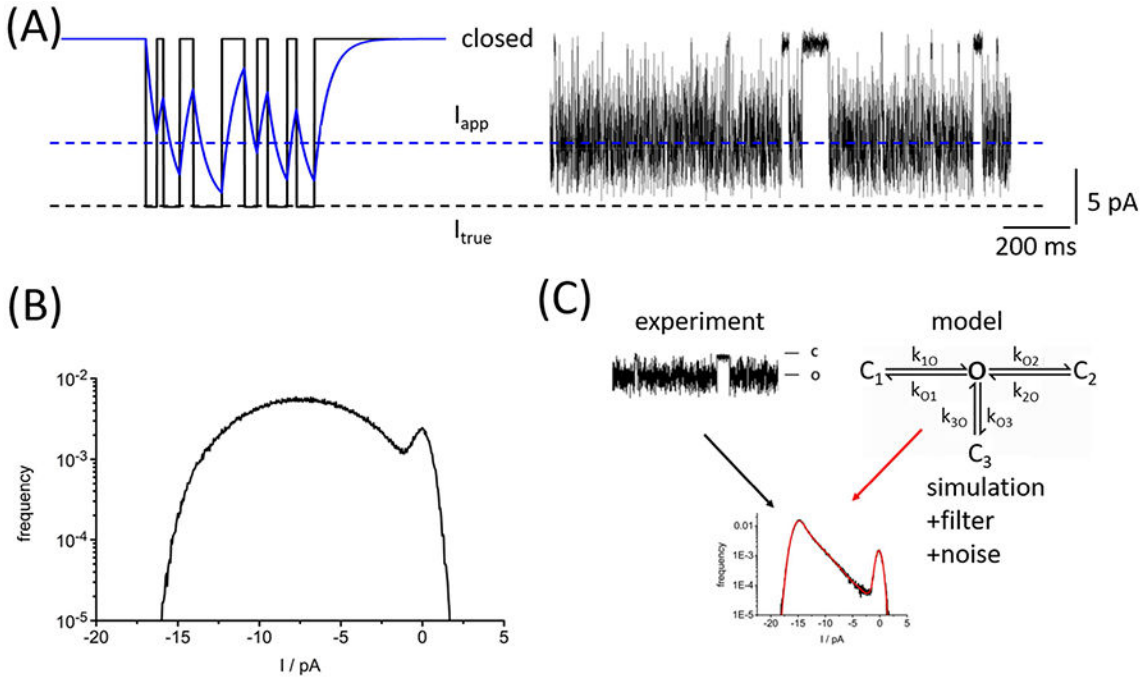

Figure 7. Analysis of fast gating with extended beta distributions.

(A) Illustration of the problem of heavily filtered data. If the gating of the channel (left-hand side in black) is faster than the recording bandwidth, the recorded signal (blue) is distorted, the true open channel current I_{true} and the individual events are no longer visible. A reduced averaged current I_{app} is recorded, the filtered gating is visible as increased open channel noise. Right-hand side: exemplary recording of a viral Kcv_{NTS} channel in a DPhPC bilayer and 100 mM KCl, pH 7 at −120 mM membrane voltage. **(B)** Representative current amplitude histogram of a recording under the same conditions as in A. The closed state at 0 mV displays Gaussian noise, whereas the apparent open state at negative currents is heavily distorted. **(C)** Scheme of the analysis with extended beta distributions. A Markov model, in this example one with one open (O) and three closed (C_1, C_2, C_3) states, is used to simulate a time series of current including low-pass filtering and noise. The resulting theoretical amplitude histogram (red) is fitted to the measured one (black).